RSC Advances

PAPER

View Article Online
View Journal | View Issue

Cite this: *RSC Adv.*, 2024, **14**, 40267

Cognitive-enhancing effect of *Cordia dichotoma* fruit on scopolamine-induced cognitive impairment in rats: metabolite profiling, *in vivo*, and *in silico* investigations†

Hagar M. Hussein, *[a] Mostafa A. Abdel Kawy,[a] Basma M. Eltanany,[b] Laura Pont,[cd] Fernando Benavente,[c] Ahmed M. Fayez,[e] Radwan Alnajjar,[fg] Ahmed A. Al-Karmalawy,[hi] Azza R. Abdelmonem[a] and Engy Mohsen[a]

Many plants are reported to enhance cognition in amnesic-animal models. The metabolite profile of *Cordia dichotoma* fruit methanolic extract (CDFME) was characterized by LC-QTOF-MS/MS, and its total phenolics content (TPC) and total flavonoids content (TFC) were determined. In parallel, its cognitive-enhancing effect on scopolamine (SCOP)-induced AD in rats was evaluated. The TPC and TFC were 44.75 ± 1.84 mg gallic acid equiv. g^{-1} sample and 5.66 ± 0.67 mg rutin equiv. g^{-1} sample, respectively. In total, 81 metabolites were identified, including phenolic acids, lignans, coumarins, amino acids, fatty acids, and their derivatives, fatty acid amides, polar lipids, terpenoids, and others. The most abundant metabolites identified were quinic acid, caffeoyl-4′-hydroxyphenyllactate, rosmarinic acid, and oleamide. CDFME (200 mg kg^{-1}) was found to significantly enhance recognition memory in the novel object recognition test. Furthermore, it nearly corrected acetylcholinesterase (AChE), acetylcholine, noradrenaline, and dopamine hippocampal levels, which changed due to SCOP. Further *in silico* validation of the *in vivo* results was conducted, focusing on the most abundant metabolites. Molecular docking showed that rosmarinic acid, caffeoyl-4′-hydroxyphenyllactate, sebestenoid C, and sagerinic acid exhibited the greatest affinity for receptor binding against AChE. However, molecular dynamics and mechanics calculations clarified that the complex of caffeoyl-4′-hydroxyphenyllactate with AChE was the most stable one. This study represents the first comprehensive metabolite profiling of CDFME to assess its cognition-enhancing effect both *in vivo* and *in silico*. These results demonstrate that CDFME protects against SCOP-induced cognitive impairment. Thus, additional preclinical and clinical studies on CDFME may provide an attractive approach in pharmacotherapy and AD prophylaxis.

Received 30th September 2024
Accepted 5th December 2024

DOI: 10.1039/d4ra06991a

rsc.li/rsc-advances

1. Introduction

Scopolamine (SCOP) is a non-selective post-synaptic muscarinic antagonist that disrupts cholinergic neurotransmission. Because it can penetrate the blood–brain barrier, SCOP is often used to cause cognitive deterioration in an experimental model to evaluate and discover anti-amnesic drugs. It impairs memory and learning in mice and humans, particularly the processes of learning acquisition and short-term memory. According to studies, Alzheimer's patients and SCOP-induced animals have similar memory problems.[1,2]

There are about 50 million people who have dementia globally.[3] Alzheimer's disease (AD) has become one of the century's biggest global health concerns, affecting millions of individuals worldwide. AD is currently considered the third leading cause of death in developed nations, behind cancer and cardiovascular disease. AD is a progressive and chronic neurodegenerative disorder that profoundly impacts cognitive

[a]*Department of Pharmacognosy, Faculty of Pharmacy, Cairo University, Cairo 11562, Egypt. E-mail: hagar.elhag@pharma.cu.edu.eg*
[b]*Department of Pharmaceutical Analytical Chemistry, Faculty of Pharmacy, Cairo University, Cairo 11562, Egypt*
[c]*Department of Chemical Engineering and Analytical Chemistry, Institute for Research on Nutrition and Food Safety (INSA-UB), University of Barcelona, Barcelona 08028, Spain*
[d]*Serra Húnter Program, Generalitat de Catalunya, Barcelona 08007, Spain*
[e]*School of Life and Medical Sciences, University of Hertfordshire Hosted by Global Academic Foundation, New Administrative Capital, Cairo 11835, Egypt*
[f]*Computer-Aided Drug Design (CADD) Unit, Faculty of Pharmacy, Libyan International Medical University, Benghazi, Libya*
[g]*Department of Chemistry, Faculty of Science, University of Benghazi, Benghazi, Libya*
[h]*Department of Pharmaceutical Chemistry, College of Pharmacy, The University of Mashreq, Baghdad 10023, Iraq*
[i]*Department of Pharmaceutical Chemistry, Faculty of Pharmacy, Horus University-Egypt, New Damietta 34518, Egypt*

† Electronic supplementary information (ESI) available. See DOI: https://doi.org/10.1039/d4ra06991a

functions such as memory, orientation, judgment, and reasoning.[4] It is characterized by dementia resulting from various pathological features, including amyloid beta plaques, glutamate excitotoxicity, neurofibrillary tangles, and hyperphosphorylated tau protein.[5] Further pathological characteristics include neuroinflammation, oxidative stress-induced cell damage, and cholinergic dysfunction. These conditions result in neurodegeneration and a loss of synapses and neurons, which results in the macroscopic atrophy of the brain areas related to memory, such as the hippocampus.[4] Cholinergic neurons release acetylcholine (ACh), a neurotransmitter that has a role in signal transduction linked to memory and learning.[6] Acetylcholinesterase (AChE) inhibitors raise synaptic ACh levels, allowing the signal to be potentiated, thus improving cognition and everyday functioning.[4] So, methods that lower the high level of AChE are thought to be effective for treating memory problems.[7]

Additionally, noradrenaline (NA) and dopamine (DA) are crucial neuromodulators involved in cognitive functions and are related to the psychological and behavioral symptoms of dementia.[8] Concerning AD treatments, current anti-AD drugs, such as donepezil (DON), rivastigmine, galantamine, and memantine, help alleviate clinical symptoms. However, these medications are associated with numerous side effects and are proven effective primarily in mild and moderate cases of AD.[3] Moreover, the complexity of AD, characterized by multiple contributing factors, challenges their efficacy. As a result, research into developing novel, potent medications for AD has gained international attention. In this regard, several natural products have gained interest in the pharmaceutical industry and the scientific research community due to their neuroprotective effects, targeting different pathological pathways related to AD.[4]

Cordia dichotoma G. Forst. (Indian cherry), a flowering tree in the Boraginaceae family, presents various medicinal properties. *C. dichotoma* produces pulpy, edible fruits with single-seed kernels encased in a transparent, viscid, sweet pulp. The fruit pulp serves various culinary purposes, being consumed fresh or raw as a spice or condiment in a variety of foods.[9] *C. dichotoma* is found in temperate regions worldwide, including South America, Central America, Mexico, West Africa, East Africa, South Asia, and Australia. *C. dichotoma* fruits are recognized for containing several bioactive phytochemicals such as pyrrolizidine alkaloids, coumarins, flavonoids, phenolic acids, carbohydrates, amino acids, tannins, saponins, terpenes, and sterols.[10] Fruits have been used for their diverse medicinal properties, encompassing antioxidant, antiulcer, analgesic, anti-inflammatory, wound-healing, demulcent, astringent, diuretic, emollient, expectorant, hepatoprotective, analgesic, antidiabetic, antibacterial, anthelmintic, anti-fertility, and aphrodisiac effects. Mucilage from *C. dichotoma* fruits is traditionally used to treat cough, fever, chest disease, uterus, and urethra disorders, while fruit kernel is used to treat tinea.[9]

In addition, *C. dichotoma* has been employed to address behavioral and memory dysfunctions, as well as psychological symptoms of dementia.[11] *Cordia myxa* leaves ethanolic extract significantly alleviated SCOP-induced cognitive impairment in mice, as measured by novel object recognition test (NORT) and passive avoidance test. Additionally, it decreases tau protein phosphorylation.[12] Additionally, *Cordia dichotoma* and *Cordia sebestena* leaves methanolic extract are reported to have *in vitro* anticholinesterase effects.[13] *Cordia dichotoma* leaves alleviate SCOP-induced AD type-dementia in mice by enhancing the cholinergic system, protecting against neuronal death in the brain, and anti-oxidant effect.[14] However, no previous study reported the cognitive function-enhancing effect of *Cordia dichotoma* fruit extract, which emphasizes the novelty of our work.[14] Given the multitude of interesting medicinal properties, there is a growing interest in employing up-to-date analytical tools to characterize such medicinal plants, aiming to understand their bioactivity and ensure their safety, quality, and efficacy. Presently, liquid chromatography-quadrupole time-of-flight tandem mass spectrometry (LC-QTOF-MS/MS) metabolomics stands out as one of the best alternatives for the untargeted metabolite profiling of plant extracts.[15–17] The reason for this is the high separation efficiency of LC and the high scanning rate, mass accuracy, and resolution of QTOF mass spectrometers, enabling the acquisition of both MS and tandem MS (MS/MS) spectra with excellent sensitivity.[18] Concerning current literature, no studies were found dealing with the elucidation and identification of the metabolite profile of CDFME and its anti-AD activity.

In this study, CDFME was profiled by untargeted LC-QTOF-MS-MS metabolomics in both negative and positive electrospray ionization (ESI) modes to characterize its bioactive compounds, and its total phenolics content (TPC) and total flavonoids content (TFC) were determined. In parallel, the cognitive-enhancing effect of CDFME on SCOP-induced cognitive impairment in rats was investigated. These alterations in rats were monitored through NORT and determinations of AChE and neurotransmitter levels in the hippocampus. To gain insights into the potential AChE inhibitory activity of the most abundant metabolites identified in CDFME, molecular docking studies were conducted, comparing their binding affinity for AChE with that of DON. Finally, the stability within the enzyme active site of the most potentially AChE inhibitory metabolites was evaluated using molecular dynamics and molecular mechanics methods.

2. Material and methods

2.1 Plant material and preparation of plant extracts

Fresh fruits (800 g) were collected from Mazhar Botanic Garden in Egypt. Fruits were authenticated by Prof. Dr Abd Haleem Abd El-Mogali, Head of the Department of Flora Researches and Plant Taxonomy at the Agriculture Research Centre, Giza, Egypt. A voucher specimen was deposited at the herbarium of the Faculty of Pharmacy, Cairo University, Cairo, Egypt (sample No. 7.9.2023). The fresh fruits were halved, and the seeds were removed. Subsequently, the pericarps were lyophilized using a Stellar laboratory freeze dryer (temp set at −40 °C, vacuum level of 100 mT) (Millrock Technology Inc., New York, NY, USA). The lyophilized dried pericarps (100 g) were extracted through the cold maceration method. The lyophilized dried pericarps were

Table 1 Percentage yield of CDFME

Plant	Solvent	Extraction method	% yield
CDFME	80% methanol	Cold maceration	6%

crushed with a blender (Toshiba, Tokyo, Japan) and then they were exhaustively extracted with 80% methanol (3 L) through repeated shaking and soaking (4 times) at room temperature over two weeks. After filtering the resultant extract, the solvent was evaporated using a rotary evaporator set to 40 °C and low pressure, yielding 6 g of brown semisolid residue of fruit extract. The dried fruit extract was kept in a freezer at −10 °C for further research.[19] The percentage yield of fruit extract is presented in Table 1.

2.2 Drugs and chemicals

Scopolamine hydrobromide was purchased from Merck (Darmstadt, Germany) and donepezil hydrochloride was obtained from Pfizer (New York, NY, USA). DON and SCOP were prepared in saline. Methanol (analytical grade) for extraction was provided by El-Gomhuria Company (Cairo, Egypt). Formic acid (≥95.0%), acetonitrile, water, and methanol (LC-MS grade) were provided by Merck.

2.3 Total phenolics and flavonoids contents

The TPC was assessed by the Folin–Ciocalteu colorimetric method.[20] Briefly, 10 μL of sample/standard was mixed with 100 μL of Folin–Ciocalteu reagent (diluted 1 : 10 v/v) in a 96-well microplate. Following the addition of 80 μL of 1 M Na_2CO_3, the mixture was allowed to sit at room temperature (25 °C) in the dark for 20 minutes. The resulting blue color was measured at 630 nm using a spectrophotometric microplate reader (FLUOstar Omega, BMG LABTECH, Ortemberg, Germany). The TPC in samples was quantified as mg gallic acid equiv. g^{-1} extract, using an external gallic acid calibration curve (25, 50, 100, 200, 400, 600, 800, and 1000 μg mL^{-1}).

The TFC was determined according to the aluminum chloride method.[21] In summary, 15 μL of the sample/standard was dispensed into a 96-well microplate, followed by the addition of 175 μL of methanol and 30 μL of 1.25% m/v $AlCl_3$. After adding 30 μL of a 0.125 M $C_2H_3NaO_2$ solution, the mixture was allowed to incubate for a duration of 5 minutes. The resulting yellow color was measured at 420 nm using the microplate reader. The TFC in samples was quantified as mg rutin equiv. g^{-1} extract using an external rutin calibration curve (1000, 500, 200, 125, 62.5, 31.4, 15.6, and 7.2 μg mL^{-1}).

2.4 LC-QTOF-MS/MS analysis

For LC-QTOF-MS/MS analysis, CDFME sample was prepared by mixing one milliliter of methanol with 10 milligrams of the extract, after which the mixture was centrifuged for 10 minutes at 13 000 × *g*, and the result was filtered through a 0.22 μm nylon syringe filter. The LC-QTOF-MS/MS experiments were carried out using a 1260 Infinity liquid chromatograph connected to a 6546 LC/QTOF mass spectrometer with an orthogonal electrospray ionization (ESI) interface (Agilent Technologies, Waldbronn, Germany). CDFME samples were analyzed in both positive and negative ESI modes, using an Agilent Technologies Zorbax SB-C18 column with dimensions of 150 mm LT × 2.1 mm ID, 5 μm particle size, and 90 Å pore diameter, and an optimized acetonitrile: water gradient (both with 0.1% v/v of formic acid) that enabled the comprehensive profiling of CDFME compounds within 25 minutes. Detailed information about the separation conditions, MS, and MS/MS measurements, as well as data processing, was as described in a previous work.[18,22]

Detected compounds were identified as metabolites based on their predicted molecular formula, accurate molecular mass, retention time (R_t), and MS/MS spectra, and by comparison with various databases (*e.g.*, KEGG, **https://www.genome.jp/kegg/compound/**, the Phytochemical Dictionary of Natural Product Database, **https://dnp.chemnetbase.com/faces/chemical/ChemicalSearch.xhtml**, Mass Bank of North America, **https://mona.fiehnlab.ucdavis.edu/**, and PubChem, **https://pubchem.ncbi.nlm.nih.gov/**), in addition to other literary sources. Therefore, the metabolites were identified at a high confidence level.

2.5 Animals

Forty adult male Wistar albino rats, weighing between 200 and 250 g (National Research Centre Giza, Egypt), were kept in cages made of polypropylene. The rats were retained together in a shared habitat with a moderate temperature of 25 ± 2 °C. Rats were given 7 days to acclimatize before starting the study. Throughout this period, regular rat pellet food and unlimited water were provided to the animals. The experiments were conducted in adherence with the "Guide for the Care and Use of Laboratory Animals" published by the US National Institutes of Health (NIH Publication No. 85-23, 2011). The research project has been approved by Cairo University's Faculty of Pharmacy Research Ethics Committee (approval number: MP (3257)).

2.6 Acute toxicity study

The lethal dose (LD_{50}) of CDFME in rats was determined adhering to the specified guidelines by the Organization for Economic Co-operation for Development (OECD, Test No. 420, 2002). Before the extract administration, rats underwent an overnight fast (12 hours) with unrestricted access to water. Just prior to the initial dosage, each rat's weight was noted. The rats were then divided into four groups of six. CDFME, suspended in saline, was orally administered to the rats at escalating doses (1000, 2000, and 4000 mg kg^{-1} body weight). The control group, kept under the same conditions, received a vehicle (saline). Over a 24 hours period, the animals were closely monitored for signs of toxicity, including draping, rising fur, excitability, tremors, salivation, twitching, and mortality. The mortality rates for each group were recorded.

2.7 SCOP-induced cognitive impairment study

2.7.1 Experimental design. Forty rats were randomly split up into five groups of eight and handled as follows: (1) control

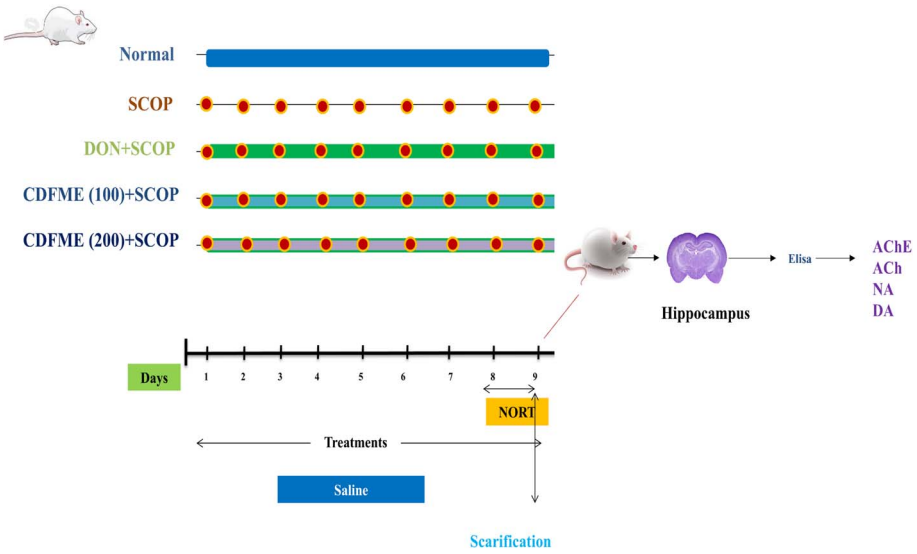

Fig. 1 Graphical representation of research protocol with grouping of animals and their daily routine.

group receiving saline; (2) SCOP-induced AD (1.14 mg kg^{-1}, i.p.); (3) DON (0.5 mg kg^{-1}, p.o.) followed by the SCOP (1.14 mg kg^{-1}, i.p.) (positive control group);[2] (4) low dose of CDFME (100 mg kg^{-1}, p.o.) followed by the SCOP (1.14 mg kg^{-1}, i.p.); and (5) high dose of CDFME (200 mg kg^{-1}, p.o.) followed by the SCOP (1.14 mg kg^{-1}, i.p.).[9] DON and CDFME were administered orally half an hour before the SCOP intraperitoneal injection. For nine days in a row, every treatment was given every day. The NORT was conducted on day 8 of the study, 30 minutes after the administration of SCOP. Upon completion of the experiment, the rats were euthanized, and their hippocampus was isolated for ensuing biochemical examination. Graphical representation of research protocol with grouping of animals and their daily routine was presented in Fig. 1.

2.7.2 Novel object recognition test. The NORT was carried out as described by a previous study by Ennaceur and Delacour (1988).[23] The test was carried out in an open black rectangular wooden box (50 × 50 × 40 cm) and consisted of three phases: habituation, training, and test. In the period of habituation, after the treatment, rats were allowed a 5 minutes exploration of the empty open field. In the training phase (T1), two similar familiar objects (blue cones) (F: a1 and a2) were positioned in different fields' corners, each 10 centimeters from the wall. Rats were positioned in the center of the open field and permitted to examine these familiar objects for 5 minutes before returning to their cages. After a 24 hours interval from T1, the test phase (T2) was initiated. In T2, a novel object (N) (a red cone) was introduced, and rats were subjected to the F and N items. The duration of exploration for each object throughout both T1 and T2, defined as the moments the rat touched the object with its nose and/or front legs, was recorded using a stopwatch. Subsequently, a discrimination index (DI) was calculated as follows:

$$DI = TN \div (TN + TF) \times 100$$

where TN and TF represent the total time spent, in both T1 and T2, exploring the N and F objects, respectively.

2.7.3 Measurement of AChE enzyme and neurotransmitters levels by ELISA. Immediately after the NORT, rats were euthanized, and their brains were removed to isolate the hippocampus, which was then stored on ice. A 100 mg portion of the hippocampus was washed with 0.01 M phosphate buffered saline to remove blood stains. Subsequently, the hippocampus was homogenized in a lysis buffer, containing 20 mM Tris (pH 8.0), 137 mM NaCl, 1% NP40, 10% glycerol, 10 mg mL^{-1} aprotinin, 1 mg mL^{-1} leupeptin, 1 mM PMSF, and 0.5 mM sodium vanadate, by means of a tissue homogenizer. Homogenates were centrifuged, and the supernatants were collected. For the determination of the different biomarkers, rat ELISA kits were employed. AChE (U mg^{-1}) and ACh (nmol mg^{-1}) levels were measured in the tissue with assay kits ab65345 and ab138871 from Abcam (Cambridge, UK), respectively. NA (ng mg^{-1}) and DA (pg mg^{-1}) levels were determined with assay kits MBS725908 and MBS269993 from MyBiosource (San Diego, CA, USA).[24]

2.8 Statistical analysis

GraphPad Prism software (version 8; GraphPad Software, Inc., San Diego, CA, USA) was used for graphical presentations and statistical analyses. The data are presented as mean ± standard deviation (SD). For data analysis, one-way ANOVA was applied, followed by Tukey's multiple comparison test. With the exception of how CDFME affects how long it takes to explore each object in the NORT, which was assessed using two-way ANOVA, followed by Sidak's multiple comparisons test. A probability level of <0.05 was deemed statistically significant for all tests conducted.

2.9 Molecular docking

The 18 most abundant metabolites identified in CDFME were docked against the AChE target receptor using the Schrödinger

2021 suite.[25] As reference standards, DON and the co-crystallized inhibitor were used. The chemical structures of these compounds were sketched with ChemDraw Professional 17.0 (Cambridge Soft Corporation., Cambridge, USA). Each structure was copied and pasted into the applied software working window, including correction of local partial charges and minimization to reach a possible local minimum energy state.[26] All the prepared structures were assembled within the same database, prepared for the next docking step. On the other hand, the target AChE enzyme's X-ray structure was obtained from the Protein Data Bank (**https://www.rcsb.org/structure/1OCE**). The enzyme structure was subjected to correction, 3D hydrogenation, and energy minimization procedures.[27]

A standardized docking procedure was conducted using the default program specifications.[28] The ideal binding pose for each examined compound was selected based on criteria like root mean square deviation (RMSD), score, and binding mode. Additionally, a validation check for the applied force field was performed by redocking the co-crystallized ligand of AChE (DON) inside AChE binding site.[29] The valid performance was verified by achieving a low RMSD value (<2 Å) and close similarities between the binding modes of both the native and redocked poses of the co-crystallized inhibitor of AChE. Finally, the binding scores for the identified metabolites were compared with those obtained for DON. Metabolites displaying the highest binding scores, indicative of their potential as AChE inhibitors, were further evaluated by molecular dynamics and molecular mechanics methods.

2.10 Molecular dynamics and molecular mechanics

Molecular dynamics simulations were conducted using the Desmond 2.2 package of the Schrödinger platform (Schrödinger, New York, NY, USA). The free energy of the bindings for the examined complexes was calculated with the same software, employing molecular mechanics with generalized Born and surface area solvation (MM-GBSA) methods. The complexes of rosmarinic acid, caffeoyl-4′-hydroxyphenyllactate, sebestenoid C, and sagerinic acid with the AChE receptor were subjected to a 200 ns simulation.[30] As a reference, the co-crystallized inhibitor (DON) complex was used. The normal physiological conditions were kept to give more reproducible results. Further details about the aforementioned methods can be found in the ESI S1 and S2.†

3. Results and discussion

3.1 Total phenolics and total flavonoids contents

Phenolic compounds are important plant components with significant redox properties. The hydroxyl groups in the structures of these compounds are essential in enabling the scavenging of free radicals, thereby contributing to their antioxidant activity.[31] TPC and TFC values were determined to complement the metabolite profiling by LC-QTOF-MS/MS, as the phenolic contents of plant extracts have been linked to the enhancement of anti-AChE activity.[9]

The TPC and TFC values in CDFME were 44.75 ± 1.84 mg gallic acid eq g^{-1} sample and 5.66 ± 0.67 mg rutin eq g^{-1} sample, respectively. These findings suggested that flavonoids constituted a minor proportion of the total phenolics in the fruit extract, suggesting that they would have a lesser impact on the bioactivity of CDFME. Graphs of gallic acid and rutin standard calibration curves were presented in Fig. S1.†

3.2 LC-MS/MS metabolite profiling

The CDFME chemical profile was analyzed using LC-QTOF-MS in both negative and positive ESI modes. The representative total ion chromatograms (TIC) of CDFME are shown in Fig. 2A and B, and the MS/MS spectra of some of the most abundant identified metabolites are illustrated in Supplementary Fig. S2–S20.† After data processing, 81 metabolites were tentatively identified depending on their R_t, predicted molecular formula, accurate molecular mass, MS/MS spectra, and cross-referencing with various databases and prior literature. Details of the annotated metabolites, including names, classes, molecular formulas, *m*/*z* of the detected molecular ions, and fragment ions are provided in Table 2.

The annotated metabolites (Table 2) pertained to numerous classes encompassing: 17 phenolic acids, 5 organic acids, 5 lignans, 3 coumarins, 5 amino acids, 12 fatty acids and their derivatives, 16 fatty acid amides, 3 polar lipids, 4 terpenoids, and 11 other compounds.

3.2.1 Phenolic acids and their derivatives. Phenolic acids are compounds having one or more hydroxyl groups and/or methoxy groups and a carboxylic acid function at the benzene ring. They derived from hydroxybenzoic acid or hydroxycinnamic. Phenolic compounds play an essential role in the resistance of plants and the control of physiological processes.[32] They are categorized into monomers and polymers (dimers, trimers, and tetramers) according to the number of phenyl moieties in their structures. Monomers of phenolic acids are characterized by the loss of CO (28 *m*/*z*), CO_2 (44 *m*/*z*), and H_2O (18 *m*/*z*), while polymers are characterized by successive or concurrent loss of $C_9H_6O_3$ (caffeoyl, 162 *m*/*z*), $C_9H_8O_4$ (caffeic acid, 180 *m*/*z*), or $C_9H_{10}O_5$ (danshensu: dihydroxyphenyl lactic acid, 198 *m*/*z*).[33] Previous investigations indicated that *C. dichotoma* fruits are rich with phenolic compounds with antimicrobial and antioxidant activities, suggesting their potential application as preservatives in the food industry.[34] In the current research, a total of 17 phenolic acids were identified in negative ESI mode (Fig. 2 and Table 2).

3.2.1.1 Hydroxy benzoic acid derivatives. Syringic acid (**15**, Fig. S2†) and syringaldehyde (**16**, Fig. S3†) (*m*/*z* 197.0454 and 181.0506, respectively, $[M–H]^-$) revealed an intense fragment ion at *m*/*z* 135, as a result of the loss of two methoxy groups $[M–H–2*(31)]^-$ and CO_2 + H_2O $[M–H–28–18]^-$, respectively. Moreover, peak **14** showed a mass difference of 162 *m*/*z* with respect to peak **15**, recommending a glucose moiety, hence was assigned as glucosyringic acid.[35] Syringic acid and syringaldehyde were previously reported in *C. dichotoma* fruit,[34] whereas glucosyringic acid was detected in the current investigation in CDFME for the first time.

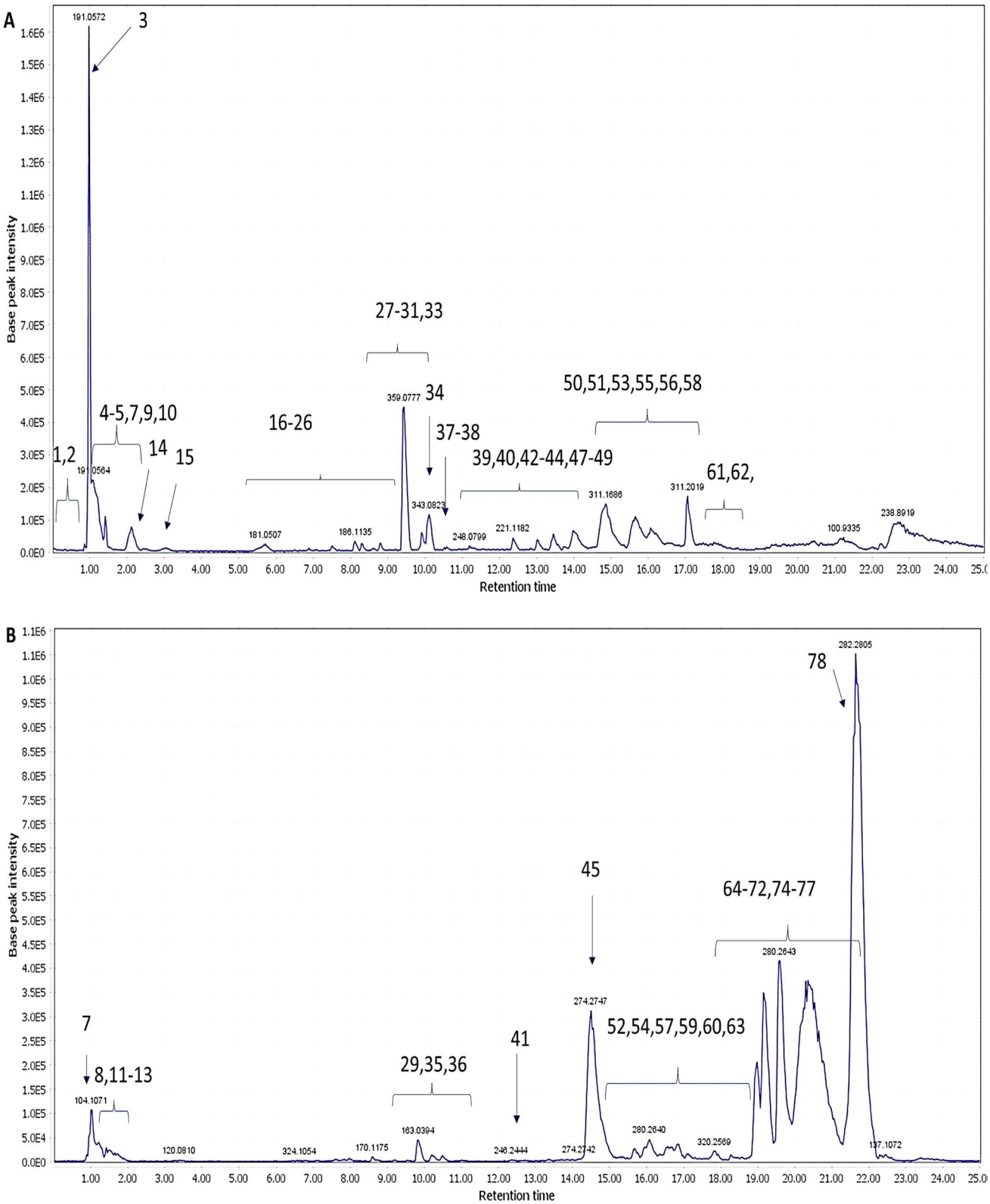

Fig. 2 LC-QTOF-MS total ion chromatograms of CDFME in negative ESI mode (A) and positive ESI mode (B). The numbers of metabolites are indicated in Table 2.

3.2.1.2 Hydroxy cinnamic acid derivatives. A total of 14 hydroxycinnamic acid derivatives were eluted between 7 and 11 minutes (Fig. 2A and Table 2). The only non-conjugated phenylethanoid detected was annotated as verbasoside (**18**).[36] Caffeic acid (**19**, Fig. S4†) (*m*/*z* 179.0349, $[M-H]^-$) presented intense fragment ions at *m*/*z* 135, 117, and 107, resulting from

Table 2 Metabolites identified in CDFME in both ESI modes

No.	R_t (min)	$[M + H]^+$	$[M-H]^-$	Error (ppm)	Formula	Proposed structure	MS/MS fragments
Hydroxybenzoic acid derivatives							
14	2.44	—	359.0982	−0.4	$C_{15}H_{20}O_{10}$	Glucosyringic acid	197, 179, 135, 123, 72
15	3.01	—	197.0454	−1.6	$C_9H_{10}O_5$	Syringic acid	179, 151, 135, 123, 117, 72
16	5.69	—	181.0506	−1.1	$C_9H_{10}O_4$	Syringaldehyde	181, 163, 135, 134, 119, 107, 72
Hydroxy cinnamic acid derivatives							
18	7.08	—	461.1654	−2.2	$C_{20}H_{30}O_{12}$	Verbasoside	461, 161, 135, 113
19	7.50	—	179.0349	−0.3	$C_9H_8O_4$	Caffeic acid	161, 135, 134, 133, 117, 107, 79
22	8.62	—	521.2023	−1.2	$C_{24}H_{26}O_{13}$	Rosmarinic acid hexoside	359, 197, 179, 161, 135, 107
24	8.97	—	717.1449	−1.6	$C_{36}H_{30}O_{16}$	Salvianolic acid B	339, 321, 295, 277, 197, 179, 109
25	9.42	—	197.0455	−0.1	$C_9H_{10}O_5$	Danshensu	179, 151, 135, 134, 123, 109, 72
27	9.55	—	359.0774	0.5	$C_{18}H_{16}O_8$	Rosmarinic acid	197, 179, 161, 135, 133, 123
30	9.91	—	163.0401	0.3	$C_9H_8O_3$	*p*-Coumaric acid	119, 103, 93
31	9.92	—	337.0928	−0.2	$C_{16}H_{18}O_8$	*p*-Coumaroylquinic acid	191, 163, 129, 119, 111, 101, 85
33	10.08	—	367.1033	−0.4	$C_{17}H_{20}O_9$	Feruloylquinic acid	193, 191, 161, 134
34	10.10	—	343.0823	0	$C_{18}H_{16}O_7$	Caffeoyl-4′-hydroxyphenyllactate	181, 179, 163, 161, 135, 133, 119
37	10.52	—	685.1555	−1.1	$C_{36}H_{30}O_{14}$	Sebestenoid C	339, 321, 295, 277, 185, 109
38	10.72	—	373.0932	0.9	$C_{19}H_{18}O_8$	Methyl rosmarinate	359, 197, 161, 150, 135, 123, 72
39	11.05	—	313.0719	−0.1	$C_{17}H_{14}O_6$	Nepetoidin B	161, 151, 133, 123, 105
40	11.34	—	313.0717	0.5	$C_{17}H_{14}O_6$	Nepetoidin B isomer	161, 151, 133, 123, 105
Organic acids							
3	0.97	—	191.0562	−0.0001	$C_7H_{12}O_6$	Quinic acid	191, 173, 171, 127, 111, 109, 85
4	0.98	—	533.1722	−0.2	$C_{19}H_{34}O_{17}$	Quinic acid + hexose$_2$	191, 171, 155, 127, 111, 85
5	1.00	—	383.1191	−1.0	$C_{14}H_{24}O_{12}$	Quinic acid derivative	191, 173, 127, 85
7	1.03	—	133.0142	−0.2	$C_4H_6O_5$	Malic acid	133, 115, 89, 71
9	1.41	—	191.0194	−1.6	$C_6H_8O_7$	Citric acid	191, 173, 155, 127, 111, 87, 85
Lignans							
20	8.29	—	521.2023	−1.0	$C_{26}H_{34}O_{11}$	Lariciresinol hexoside	359, 329, 299, 205, 187, 175
21	8.32	—	567.2080	−0.5	$C_{27}H_{36}O_{13}$	Dehydrodehyrodiconiferyl glycoside derivative	359, 341, 329, 299, 205, 187
26	9.42	—	719.1622	−0.6	$C_{36}H_{32}O_{16}$	Sagerinic acid	359, 197, 179, 161, 135, 123, 72
28	9.72	—	717.1449	−1.2	$C_{36}H_{30}O_{16}$	Rabdosiin	537, 339, 321, 295, 279, 249, 185
32	9.98	—	491.0976	−1.5	$C_{26}H_{20}O_{10}$	Globoidnan A	491, 311, 267, 197, 135
Coumarins							
29	9.82	163.0394	161.0242	2.5	$C_9H_6O_3$	Hydroxycoumarin	161, 133, 117, 115, 105, 77 163, 145, 135, 117, 107, 89, 77
35	10.28	147.0440	—	0.5	$C_9H_6O_2$	Coumarin	149, 119, 101, 91, 71, 65
36	10.46	177.0549	—	1.5	$C_{10}H_8O_3$	Methoxy coumarin	177, 162, 149, 145, 134, 135, 117, 89
Amino acids							
8	1.40	280.1396	—	1.8	$C_{11}H_{21}NO_7$	Hexosyl valine	262, 244, 216, 198, 150, 118, 84, 72
10	1.41	—	290.0878	−1.1	$C_{11}H_{17}NO_8$	Hexosyl pyroglutamate	200, 128, 101, 84
11	1.47	130.0502	128.0352	2.4	$C_5H_7NO_3$	Pyroglutamic acid	128, 102, 82, 79 130, 84, 71, 56

Table 2 (*Contd.*)

No.	R_t (min)	$[M + H]^+$	$[M-H]^-$	Error (ppm)	Formula	Proposed structure	MS/MS fragments
12	1.63	294.1553	—	1.9	$C_{12}H_{23}NO_7$	*N*-Hexosyl isoleucine	294, 230, 132, 212, 116, 112, 86, 69
13	1.71	132.1021	—	1.3	$C_6H_{13}NO_2$	Isoleucine or leucine	86, 69, 62, 56
Fatty acids and their derivatives							
41	12.33	246.2432	—	0.3	$C_{14}H_{31}NO_2$	*N*-Decyl diethanolamine	246, 228, 106, 102, 88, 71, 70, 57
42	13.45	—	721.3646	−0.8	$C_{34}H_{58}O_{16}$	Palmitoleic linolenic glucoside	397, 277, 255, 235
45	14.48	274.2748	—	2.6	$C_{16}H_{35}NO_2$	*N*-Lauryldiethanolamine (*N*-Dodecyl diethanolamine)	274, 256, 212, 106, 102, 88, 70, 57
46	14.62	230.2483	—	1.9	$C_{14}H_{31}NO$	Lauramine oxide	230, 212, 85, 71, 62, 58, 57
47	14.65	—	699.3782	−3.8	$C_{32}H_{60}O_{16}$	Palmitic oleic glucoside	397, 255, 89, 71, 57
48	14.78	—	559.3121	−1.7	$C_{28}H_{48}O_{11}$	Dirhamosyl linolenic acid	415, 277, 253, 101, 59
51	15.66	—	483.2724	−5.6	$C_{29}H_{40}O_6$	Palmitic acid derivative	483, 255, 271, 227, 153
54	16.40	230.2485	—	1.0	$C_{14}H_{31}NO$	Lauramine oxide isomer	230, 212, 71, 62, 58, 57
57	16.81	296.2588	—	1.3	$C_{18}H_{33}NO_2$	Linoleylhydroxamate	251, 169, 109, 95, 93, 57, 55
59	17.13	296.2580	—	1.5	$C_{18}H_{33}NO_2$	Linoleylhydroxamate isomer	251, 169, 109, 95, 93, 67, 57, 55
62	18.38	279.2322	277.2169	−1.4	$C_{18}H_{30}O_2$	Linolenic acid	277, 219, 188, 155, 127, 109, 83 279, 153, 149, 135, 123, 109, 83,69, 57
63	18.64	279.2321	—	0.8	$C_{18}H_{30}O_2$	Linolenic acid isomer	153, 135, 121, 109, 95, 67, 57
Fatty acid amides							
52	16.08	280.2637	—	0.7	$C_{18}H_{33}NO$	Linoleamide	263, 245, 109, 95, 69, 55
60	18.29	278.2483	—	1.2	$C_{18}H_{31}NO$	Linoleamide	243, 149, 135, 109, 95, 81, 67, 55
64	18.95	228.2328	—	3.0	$C_{14}H_{29}NO$	Myristamide (tetradecanamide)	228, 172, 116, 102, 88, 74, 57
65	19.22	254.2484	—	2.1	$C_{16}H_{31}NO$	Palmitoleamide	237, 142, 149, 135, 128, 97, 83, 69, 55
66	19.58	280.2641	—	2.1	$C_{18}H_{33}NO$	Linoleamide isomer	280, 263, 245, 109, 95, 69, 55
67	19.84	242.2484	—	2.6	$C_{15}H_{31}NO$	Pentadecanamide	242, 200, 116, 102, 88, 57
68	20.00	284.2951	—	1.0	$C_{18}H_{37}NO$	Octadecanamide	284, 242, 228, 116, 102, 88, 71, 57
69	20.21	242.2832	—	1.8	$C_{15}H_{31}NO$	Pentadecanamide isomer	242, 200, 116, 102, 88, 57
71	20.28	268.2640	—	1.8	$C_{17}H_{33}NO$	Heptadecenamide	268, 233, 226, 149, 121, 97, 83, 69, 55
72	20.44	338.2679	—	3.1	$C_{22}H_{43}NO$	Erucamide	321, 149, 67, 57
75	21.11	310.3110	—	1.7	$C_{20}H_{39}NO$	Eicosenamide	310, 268, 149, 135, 121, 97, 83, 69, 57
76	21.32	256.2640	—	1.9	$C_{16}H_{33}NO$	Palmitamide (hexadecanamide)	256, 128, 116, 102, 88, 71, 57
77	21.45	284.2953	—	1.7	$C_{18}H_{37}NO$	Octadecanamide isomer	284, 242, 228, 116, 102, 88, 71, 57
78	21.89	282.2802	—	3.7	$C_{18}H_{35}NO$	Octadecenamide (oleamide)	265, 247, 149, 135, 121, 97, 83, 69, 57
79	21.81	537.5359	—	1.0	$C_{34}H_{68}N_2O_2$	Palmitamide derivative	282, 256, 212, 135, 102, 97, 83, 69, 57
80	21.85	256.2642	—	2.7	$C_{16}H_{33}NO$	Palmitamide (hexadecanamide) isomer	256, 116, 102, 88, 71, 57
Polar lipids							
43	13.49	—	555.2839	−1.0	$C_{25}H_{48}O_{11}S$	SQMG (16 : 0)	555, 299, 255, 225, 207, 165, 81
53	16.32	—	815.4977	−0.9	$C_{43}H_{76}O_{12}S$	SQDG (16 : 0; 18 : 3)	815, 559, 277, 255, 225, 207, 165, 81
56	16.80	—	833.5177	−1.0	$C_{43}H_{79}O_{13}P$	Diacyl phosphatidyl-myoinositol (16 : 0/18 : 2)	833, 279, 255, 241, 153, 81,79
Terpenoids							
17	6.49	—	443.1921	−0.3	$C_{21}H_{32}O_{10}$	Penstemide	443, 113, 101, 71, 59
55	16.64	—	347.1707	−1.2	$C_{16}H_{28}O_8$	Rhodiolosides A (monoterpene)	301, 285, 217

Table 2 (*Contd.*)

No.	R_t (min)	$[M+H]^+$	$[M-H]^-$	Error (ppm)	Formula	Proposed structure	MS/MS fragments
73	20.44	621.3082	—	3.3	$C_{36}H_{44}O_9$	Diterpene benzoate triacetate	621, 561, 533, 515, 505, 461, 433, 193
81	21.89	621.3087	—	2.5	$C_{36}H_{44}O_9$	Diterpene benzoate triacetate isomer	621, 561, 533, 505, 461, 433, 193
Other compounds							
1	0.95	—	387.1139	−1.3	$C_{13}H_{24}O_{13}$	Disaccharide derivative (carbohydrate)	191, 179, 119, 101, 89, 71, 59
2	0.96	—	341.1086	−1.5	$C_{12}H_{22}O_{11}$	Hexose-pentose	127, 119, 101, 89, 71, 59
6	1.02	104.1071	—	0.8	$C_5H_{13}NO$	Choline (nitrogenous compound)	105, 104, 60, 59, 58
23	8.79	—	623.1613	−0.7	$C_{28}H_{32}O_{16}$	Isorhamnetin 3-*O*-rutinoside (narcissin)	623, 315, 314, 299, 255, 151, 107
44	14.02	—	297.1526	−1.2	$C_{16}H_{26}O_3S$	*p*-Decylbenzenesulfonic acid	297, 225, 183, 182, 161, 119
49	14.82	—	311.1686	0	$C_{17}H_{28}O_3S$	Undecylbenzenesulfonic acid	311, 225, 197, 183, 170, 119
50	15.64	—	325.1838	−1.1	$C_{18}H_{30}O_3S$	Dodecylbenzenesulfonic acid	325, 297, 183, 170, 119
58	17.05	—	311.2013	−1.1	$C_{21}H_{28}O_2$	Bisphenol G (hydrocarbons)	183, 149, 134, 133
61	18.33	391.2849	—	1.5	$C_{24}H_{38}O_4$	Dioctyl phthalate (hydrocarbons)	291, 167, 149, 71
70	20.22	593.2769	—	0.7	$C_{35}H_{36}N_4O_5$	Pheophorbide A (chlorophyll derivatives)	533, 505, 461, 447, 433
74	20.70	593.2759	—	2.2	$C_{35}H_{36}N_4O_5$	Pheophorbide A isomer (chlorophyll derivatives)	593, 533, 505, 461, 447, 433

the loss of CO_2 $[M-H-44]^-$, $CO_2 + H_2O$ $[M-H-44-18]^-$, and $CO + CO_2$ $[M-H-28-44]^-$, respectively. The mass spectra of peaks **34** (*m*/*z* 343.0810, $[M-H]^-$) and **39** (*m*/*z* 313.0719, $[M-H]^-$) presented an intense fragment ion at *m*/*z* 161 related to the dehydrated caffeic acid moiety, indicating a caffeic acid derivative. Peak **34** was annotated as caffeoyl-4′-hydroxyphenyllactate (Fig. S7†),[37] while, peak **39** was annotated as nepetoidin B (Fig. S9†), which is a caffeic acid ester.[38]

Rosmarinic acid (**27**, Fig. S6†) (*m*/*z* 359.0774, $[M-H]^-$) was readily characterized by its fragment ions at *m*/*z* 179 and 197, corresponding to caffeic acid and danshensu moieties, respectively. Peaks **22** and **38** presented a mass difference of 162 and 15 *m*/*z* in comparison to peak **27**, indicating an extra hexose and methyl group moiety, respectively, hence they were annotated as rosmarinic acid hexoside and methyl rosmarinate, respectively.[37]

Regarding peak **24** (Fig. S5†) (*m*/*z* 717.1449, $[M-H]^-$), it was identified as salvianolic acid B. Its mass spectrum revealed characteristic fragment ions at *m*/*z* 339 and 321 resulting from the loss of danshensu + caffeic acid $[M-H-198-180]^-$ and two danshensu moieties $[M-H-2*198]^-$, respectively.[37] Sebestenoid C (**37**, Fig. S8†) (*m*/*z* 685.1555, $[M-H]^-$), presented fragment ions at *m*/*z* 321 $[M-H-C_{18}H_{18}O_7-H_2O]^-$ and 295 $[M-H-C_{18}H_{18}O_7$-carboxy group$]^-$.[39] Finally, the rest of the phenolic acids were annotated as danshensu (**25**),[37] *p*-coumaric (**30**) acid, *p*-coumaroylquinic acid (**31**), and feruloylquinic acid (**33**), respectively.[40]

It is noteworthy that rosmarinic acid and caffeoyl-4′-hydroxyphenyllactate were found to be the most abundant phenolic acids identified. Additionally, all of the previous phenolic acids, except caffeoyl-4′-hydroxyphenyllactate, salvianolic acid B, sebestenoid C, and nepetoidin B, had been previously reported in *C. dichotoma* fruit.[34] Meanwhile, sebestenoid C and nepetoidin B were previously reported in *Cordia sebestena* fruit.[39]

3.2.2 Organic acids. Organic acids are organic compounds with acidic characteristics, classified according to the number of carboxylic groups. Plant cells use them as intermediates in major carbon metabolism, and they are engaged in numerous metabolic processes, including the tricarboxylic acid cycle, glycolysis, and photorespiration.[32] Furthermore, several authors have referred to naturally occurring organic acids in plants and other sources as lifespan essentials, which can prevent neurodegenerative diseases, including AD, and promote healthy aging.[41]

Quinic acid (**3**, Fig. S10†), quinic acid derivatives (**4** and **5**),[42] malic acid (**7**), and citric acid (**9**) were identified in CDFME (Fig. 2A and Table 2). Quinic acid was the most abundant organic acid identified. Their mass spectra revealed abundant fragment ions due to the loss of CH_2, CO_2, CO, and H_2O groups (14, 44, 28, and 18 *m*/*z*, respectively).[32,37]

3.2.3 Lignans. Lignans are produced *via* the shikimic acid biosynthesis pathway. They are formed by a β–β′ (8–8′) linkage between two phenylpropane units (C6–C3) with a variable degree of oxidation in the side chain and a characteristic pattern of substitution in the aromatic moiety. They function as antifeedants, safeguarding seeds and plants against herbivores.

They have numerous biological activities, including antitumor, hypolipidemic, antiviral, anti-inflammatory, and estrogenic activities.[43]

Five lignans (Fig. 2A and Table 2) (**20**, **21**, **26**, **28**, and **38**), not previously reported in *C. dichotoma*, were identified in negative ESI mode. Lariciresinol hexoside (**20**) (*m*/*z* 521.2023, $[M–H]^-$) revealed fragment ions at *m*/*z* 359 and 329 after the loss of a hexose sugar $[M–H–162]^-$ and a hexose sugar plus two methyl groups $[M–H–162–15–15]^-$, respectively.[44] Neolignane dihydrodehyrodiconiferyl glycoside derivative (21) was also annotated.[40] Neolignans had been previously isolated from *Cordia americana*.[45] Sagerinic acid (**26**, Fig. S11†) (*m*/*z* 719.1622, $[M–H]^-$), a possible dimer of rosmarinic acid, showed a fragment ion at *m*/*z* 359 after the loss of $C_{18}H_{16}O_8$ $[M–H–360]^-$, as reported in previous studies.[46] Rabdosiin (**28**) (*m*/*z* 717.1449, $[M–H]^-$), and globoidnan A (**32**, Fig. S12†) (*m*/*z* 491.0976, $[M–H]^-$) with an arylnaphthalene-type lignan skeleton were also identified, which were previously reported in *Cordia rufescens*.[47] They showed fragmentation patterns characterized by the neutral losses of caffeic acid (−180 *m*/*z*) or danshensu (−198 *m*/*z*) and carboxyl groups (−44 *m*/*z*), which are present in their structures.[48]

3.2.4 Coumarins. Coumarins, a group of plant-derived secondary metabolites with benzo-α-pyranone parent nucleus, are known for their role in iron absorption and potential in combating bacterial and viral infections. They also display a wide range of biological properties, such as antiviral, antibacterial, antidiabetic, antioxidant, and anti-inflammatory activities.[49] Peaks **29** (Fig. S13†), **35**, and **36** (Fig. S14†) (Fig. 2 and Table 2) were annotated as hydroxycoumarin, coumarin, and methoxy coumarin, respectively. Coumarins displayed characteristic fragment ions by losing 28, 44, 56, 72, and 18 *m*/*z* units, attributed to the loss of neutral molecules such as CO, CO_2, (CO + CO), (CO + CO_2), and H_2O, respectively.[50] Coumarins were massively reported in genus *Cordia*.[51]

3.2.5 Amino acids. Amino acids consist of a specific side chain, a carboxyl group (COOH), an amino group (NH_2), and a core carbon atom known as the α-carbon.[32] They are essential signaling molecules in plants that regulate root and shoot architecture, flowering time, and stress defense.[52] Amino acids are essential for protein synthesis, cell growth, differentiation, function, and neurotransmitter production in the brain.[53]

Sugar conjugates of amino acids, including hexosyl valine (**8**) (*m*/*z* 280.1396, $[M + H]^+$), hexosyl pyroglutamate (**10**) (*m*/*z* 290.0878, $[M–H]^-$), and hexosyl isoleucine (**12**) (*m*/*z* 294.1553, $[M + H]^+$), exhibited similar fragmentation behavior, involving the loss of the attached sugar unit and formation of a base peak at *m*/*z* 118, 128, and 132, in metabolites **8**, **10**, and **12**, respectively. Additionally, the typical amino acid fragments were observed, indicating the loss of NH_3, H_2O, CO, CO_2, and HCOOH groups (17, 18, 28, 44, and 46 *m*/*z* units, respectively).[32,54] These amino acid sugar conjugates are reported here for the first time in CDFME. Additionally, pyroglutamic acid (**11**, Fig. S15†) and isoleucine or leucine (**13**, Fig. S16†) were identified.[32]

3.2.6 Fatty acids and their derivatives. Fatty acids, consisting of 12–24 carbon chains with a COOH group at one end, are essential structural components of lipids, plant cell membranes, and certain bioactive compounds.

Most fatty acid fragmentations revealed neutral water loss(es) followed by decarboxylation.[32] Eight fatty acids and their derivatives were identified in positive and/or negative ESI mode (Fig. 2 and Table 2). They are namely palmitoleic linolenic glucoside (**42**), palmitic oleic glucoside (**47**),[46] dirhamnosyl linolenic acid (**48**),[55] palmitic acid derivative (**51**),[46] linoleylhydroxamate (**57**), linoleylhydroxamate isomer (**59**),[56] linolenic acid (**62**), and linolenic acid isomer (**63**).[32]

Unsaturated fatty acids, such as linolenic acid and its derivatives (**42**, **48**, **57**, **59**, **62**, and **63**), are vital nutrients with a variety of physiological benefits, including neuroprotective, antioxidant, and anti-inflammatory actions.[57] Additionally, four fatty acid nitrogenous derivatives were also identified, namely, *N*-decyl diethanolamine (**41**), *N*-decyl diethanolamine (**45**), lauramine oxide (**46**), and lauramine oxide isomer (**54**).[54] Many studies have reported the presence of various fatty acids in *C. dichotoma* seeds, including linoleic acid, oleic acid, and palmitic acid.[9] However, to the best of our knowledge, dirhamnosyl linolenic acid and linoleylhydroxamate, were detected here for the first time in CDFME.

3.2.7 Fatty acid amides. Fatty acid amides are a type of lipid bioregulator formed by the amidation of the corresponding amines by long-chain saturated and unsaturated fatty acids. They have a vital function in robust plant–microbe interactions, targeting protein synthesis and causing leakage of intracellular components. As therapeutic agents, fatty acid amides have a wide range of potential applications, including inflammation, cancer, parasitic or bacterial infections, obesity, and diabetes.[58]

Sixteen fatty acid amides were identified in positive ESI mode (Fig. 2B and Table 2). These compounds produced main fragment ions of $[M + H–NH_3]^+$ and $[M + H–NH_3–H_2O]^+$, indicating ammonia and ammonia plus water losses at the carboxamide functional group. Additionally, all fatty acyl moieties displayed consecutive losses of 14 *m*/*z* units, indicative of an acyl chain.[57] For instance, peak **65** (Fig. S17†) (*m*/*z* 254.2484, $[M + H]^+$) revealed fragment ions at *m*/*z* 237 $[M + H–NH_3]^+$, 142 $[M + H–C_8H_{16}]^+$, and 128 $[M + H–C_9H_{18}]^+$ and was annotated as palmitoleamide. Similarly, the mass spectrum of octadecenamide (**78**, Fig. S18†) (*m*/*z* 282.2802, $[M + H]^+$) showed fragment ions at *m*/*z* 265 $[M + H–NH_3]^+$ and 247 $[M + H–NH_3–H_2O]^+$.

Finally, peaks **52**, **60**, **64**, **66**, **67**, **68**, **69**, **71**, **72**, **75**, **76**, **77**, **79**, and **80** were annotated as linoleamide, linolenamide, myristamide, linoleamide isomer, pentadecanamide, octadecanamide, pentadecanamide isomer, heptadecenamide, erucamide, eicosenamide, palmitamide, octadecanamide isomer, palmitamide derivative, and palmitamide isomer, respectively.[57,59] Fatty acid amides were found to be one of the most abundant class of metabolites detected in positive ESI mode and were identified here for the first time in CDFME.

3.2.8 Polar lipids. Polar lipids, which are amphiphilic lipids with hydrophilic and hydrophobic regions, play crucial roles in plants as signaling mediators, energy storage, and cell membrane structural elements.[18] Major classes of polar lipids include phospholipids, glycolipids, sphingolipids, and other derivatives.

Two sulfoglycolipids and one phospholipid were identified in the negative ESI mode (Fig. 2A and Table 2). Sulfolipids are a class of lipids in which a sulfated sugar (mostly quinovose or glucose) is bonded to acylglycerol. Peaks **43** and **53**, with $[M–H]^-$ at *m*/*z* 555.2839 and 815.4977, were identified as sulfoquinovosyl-monoacylglycerol (SQMG) (16 : 0) and sulfoquinovosyl-diacylglycerol (SQDG) (16 : 0; 18 : 3), respectively. Sulfolipids showed characteristic fragment ions at *m*/*z* 225 (sulfoquinovosyl-18) and 81 (sulfonate). SQMG (16 : 0) also featured a fragment ion at *m*/*z* 255 related to a palmitic acid moiety (16 : 0). Similarly, SQDG (16 : 0; 18 : 3) displayed fragments at *m*/*z* 255 and 277 related to palmitic acid (16 : 0) and linolenic acid moieties (18 : 3), respectively.[57] Regarding the identified phospholipid, peak **56** [*m*/*z* 833.5177, $[M–H]^-$] was annotated as diacyl phosphatidyl-myoinositol. It revealed fragment ions at *m*/*z* 241 (phospho-myoinositol), 153 (phosphoglycerol), 81 (sulfonate), and 79 (phosphonate).[18] To the best of our knowledge, polar lipids were detected here for the first time in CDFME.

3.2.9 Terpenoids. Terpenoids are a class of natural compounds that are derived from mevalonic acid (MVA), which are made up of a plurality of isoprene (C5) structural units. They are essential for the physiological functions, environmental reactions, and growth and development of plants. Terpenoids demonstrate a broad spectrum of biological properties, including antimicrobial, anti-inflammatory, antioxidant, anticancer, and antiallergic effects.[60]

Four terpenoid compounds were identified in positive ESI (Fig. 2B and Table 2). Peaks **17** and **55** were annotated as penstemide (iridoid-type glucoside)[56] and rhodioloside A,[61] respectively. Peaks **73** and **81** (621.3082 and 621.3087, respectively, $[M + H]^+$) were annotated as diterpene acetate ester isomers. Their fragmentation was characterized by the neutral loss of an acetic acid unit (−60 *m*/*z*), but their exact structure could not be conclusively determined.[62]

3.2.10 Other phytochemical classes. Other compounds, belonging to phytochemicals distinct from those mentioned above, were identified in both positive and/or negative ESI modes (Fig. 2 and Table 2). The mass spectrum of peak **6** (Fig. S19†) (*m*/*z* 104.1072, $[M + H]^+$) revealed an intense fragment ion at *m*/*z* 60 associated with the release of a trimethylammonium cation $[(C_3H_{10}–N)]^+$, and it was annotated as choline.[63] In this study, only one flavanol was detected in negative ESI mode. The MS/MS spectrum of peak **23** (Fig. S20†) (*m*/*z* 623.1613, $[M–H]^-$) revealed a base fragment ion at *m*/*z* 315 (isorhamnetin) due to the loss of the attached rutinose moiety $[M–H–308]^-$, confirming the identification of isorhamnetin-3-*O*-rutinoside.[40]

Several sulfonic acids (**44**, **49**, and **50**)[35] and two chlorophyll derivatives [pheophorbide (**70**) and pheophorbide isomer (**74**)] were identified in our study.[64] As far as we know, choline and these sulfonic acids were identified here for the first time in CDFME.

3.3 Acute toxicity study

The therapeutic application of plant medicines without scientific evidence about their toxicity profile may raise serious concerns. To ensure the safety of plant medicines for human use, toxicity testing is typically conducted on various animal models. No toxicity signs (such as hypoactivity, coma, convulsions, diarrhea, respiratory depression, perspiration, salivation, and alteration in the locomotor activity) or deaths were recorded following oral administration of CDFME at doses of 1000 and 2000 mg kg^{-1} compared to the control group. However, at a dose of 4000 mg kg^{-1}, there was a 33.3% mortality rate. Overall, CDFME exhibited a low toxicity profile, and doses of 100 and 200 mg kg^{-1} were selected for further *in vivo* evaluation.

3.4 Cognitive-enhancing effect of CDFME

SCOP is an anticholinergic drug known to block muscarinic receptors and act as a muscarinic receptor antagonist. The antagonistic role of SCOP causes significant deficiencies in attention and memory. The SCOP-induced dementia model has been extensively used to assess possible treatment drugs for treating AD. AD is a brain disease that gradually decreases thinking and memory capacities, as well as the ability to do even the most fundamental tasks.[2] To investigate the cognitive-enhancing effect of CDFME in rats, learning and memory were assessed using the NORT and various biochemical parameters related to memory function were measured. These included the measurement of the hippocampal levels of AChE enzyme and neurotransmitters (ACh, NA, and DA). Additionally, the results of these *in vivo* investigations were assessed in relation to the metabolite profile established by LC-QTOF-MS/MS. Table 3 shows the DI in the NORT, as well as the levels of AChE, ACh, NA, and DA in the different rat groups.

3.4.1 NORT. The NORT served as a behavioral model to evaluate memory and learning through visual recognition, which is affected in the early stages of AD. Research suggests that the integrity of the hippocampus and cerebral cortex is essential in this form of recognition memory. Enhanced recognition memory and exploratory learning are indicated by

Table 3 Discrimination index (DI) in the NORT and levels of AChE, ACh, NA, and DA in the different rat groups

Group	DI	AChE (U mg^{-1})	ACh (nmol mg^{-1})	NA (pg mg^{-1})	DA (ng mg^{-1})
Normal	0.83 ± 0.02	0.21 ± 0.02	5.100 ± 0.49	3.78 ± 0.74	16.49 ± 1.81
SCOP (1.14 mg kg^{-1})	0.53 ± 0.03	0.91 ± 0.01	1.200 ± 0.23	21.96 ± 1.05	45.06 ± 4.73
DON (0.5 mg kg^{-1}) + SCOP	0.77 ± 0.17	0.17 ± 0.02	4.900 ± 0.20	6.53 ± 0.73	19.97 ± 1.51
CDFME (100 mg kg^{-1}) + SCOP	0.52 ± 0.02	0.84 ± 0.02	1.200 ± 0.25	20.26 ± 0.98	41.58 ± 1.95
CDFME (200 mg kg^{-1}) + SCOP	0.73 ± 0.03	0.40 ± 0.03	4.500 ± 0.76	10.20 ± 0.65	26.26 ± 2.34

a higher percentage of the duration spent with the new object.[65] Fig. 3A demonstrates a substantial decrease ($p < 0.05$) in time spent with the novel item in the SCOP control group in comparison to the normal control group. Additionally, in the DON and CDFME (200 mg kg^{-1}) groups, time spent with the new object N increased significantly ($p < 0.05$) compared to the SCOP control group. These trends can be clearly observed in Fig. 3A, where the DI is represented for the different groups of rats. As can be observed, SCOP significantly reduced the DI by 37% compared to the normal control group. Controversy, treatments with DON and CDFME (200 mg kg^{-1}) increased the DI by 47% and 39%, respectively, when compared to the SCOP control group. Furthermore, the effect of CDFME at a dose of 100 mg kg^{-1} was statistically insignificant (Table 3 and Fig. 3B). Therefore, these outcomes suggested that CDFME had an anti-amnesic effect in rats with SCOP-induced cognitive impairment.

Various phytoconstituents identified in CDFME may contribute to the observed cognitive enhancement effect. Specifically, phenolic acids, including salvianolic acid B, caffeic acid, rosmarinic acid, syringic acid, *p*-coumaric acid, and danshensu, have been reported to improve cognitive abilities in *in vitro* and *in vivo* animal models of AD.[66,67] Essential amino acids have a potential role in enhancing human learning, memory, and neuro-cognitive performance.[68] Additionally, administering oleamide to mice enhanced their learning and memory-related skills.[69] Fatty acids like linolenic acid have also been reported to increase DI in rats in the NORT in *in vivo* animal models.[70] Furthermore, phospholipids reversed SCOP-induced spatial memory deficits in mice.[71]

3.4.2 AChE and neurotransmitter levels (ACh, NA, and DA). ELISA was used as a simple, quick, and sensitive approach to measure AChE and neurotransmitters in the hippocampus of rats.[72] The cholinergic neurotransmission system in the basal forebrain plays a crucial role in memory and learning, underscoring the importance of maintaining ACh levels for proper brain function. Furthermore, memory disorders in AD may be caused by disruption to the brain's cholinergic pathways. Additionally, elevated AChE activity results in increased ACh degradation, subsequently reducing the ACh pool in rat hippocampal tissues. AChE inhibitors are now considered the most potential medication for AD, as they enhance the viability of ACh in central cholinergic synapses.[73] Indeed, one of the main reasons for cholinergic deficits following SCOP administration is the increase in AChE activity and the subsequent decrease in ACh levels.[2,65] The results obtained (Table 3 and Fig. 4) confirmed that SCOP increased AChE levels in comparison to the normal control group (by 333%). While treatments with DON and CDFME at a dose of 200 mg kg^{-1} lowered the AChE levels by 81% and 56%, respectively, in comparison to the SCOP control group. On the other hand, CDFME (100 mg kg^{-1}) resulted in no meaningful effect. Moreover, treatment with SCOP lowered ACh level by 76% compared to the normal control group, and these lower levels were maintained with the treatment of CDFME (100 mg kg^{-1}). In contrast, treatments with DON and CDFME (200 mg kg^{-1}) increased ACh level by 308% and 275%, respectively, compared to the SCOP control group.

Various metabolites identified in CDFME have anti-AChE effect and restore ACh levels. Phenolic compounds, such as caffeic acid, syringic acid, lariciresinol,[74] salvianolic acid B, and

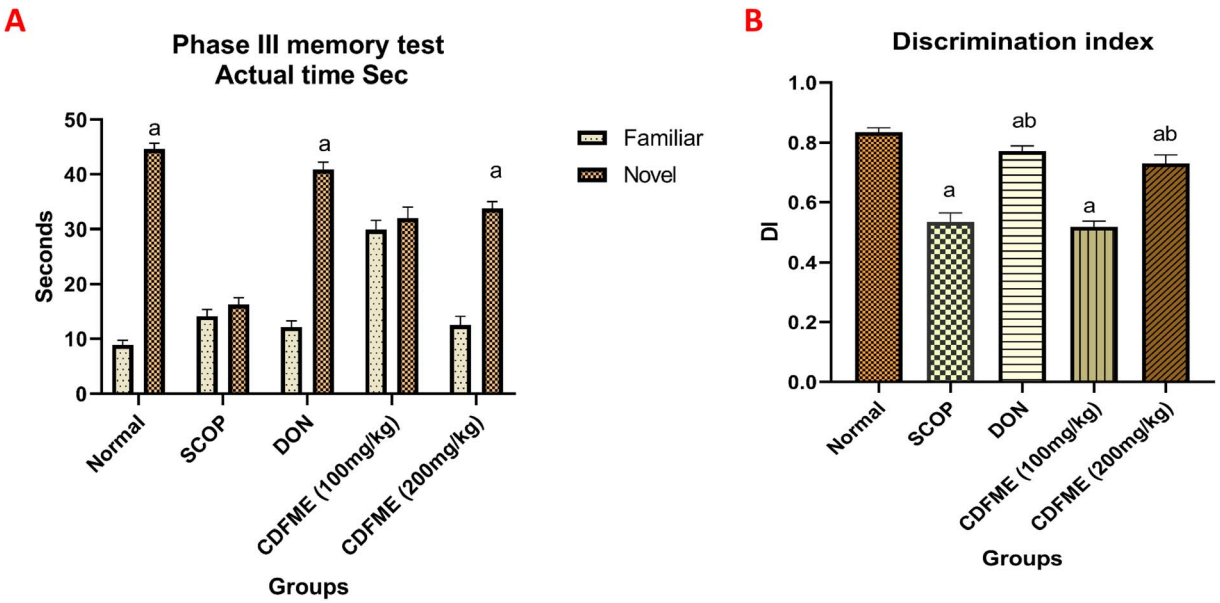

Fig. 3 (A) Effect of CDFME on the exploring time of the two different objects. Each bar represents the mean ± SD ($n = 8$). Statistical analysis was conducted using two-way ANOVA, followed by Sidak's multiple comparisons test. The letter "a" indicates significant differences for the exploration of the novel new object *versus* the familiar one ($p < 0.05$). (B) Effect of CDFME on the DI. Each bar represents the mean ± SD ($n = 8$). Statistical analysis was conducted by one-way ANOVA, followed by the Tukey multiple comparison test. Letters "a" and "b" indicate significant differences in the DI in comparison to the normal control group and the SCOP control group ($p < 0.05$), respectively. The findings indicated significant variations in memory performance across groups (df between groups = [4], df within groups = [35], R^2 = [0.98]), particularly with the 200 mg kg^{-1} dose of CDFME, which showed an effect approaching that of the standard treatment.

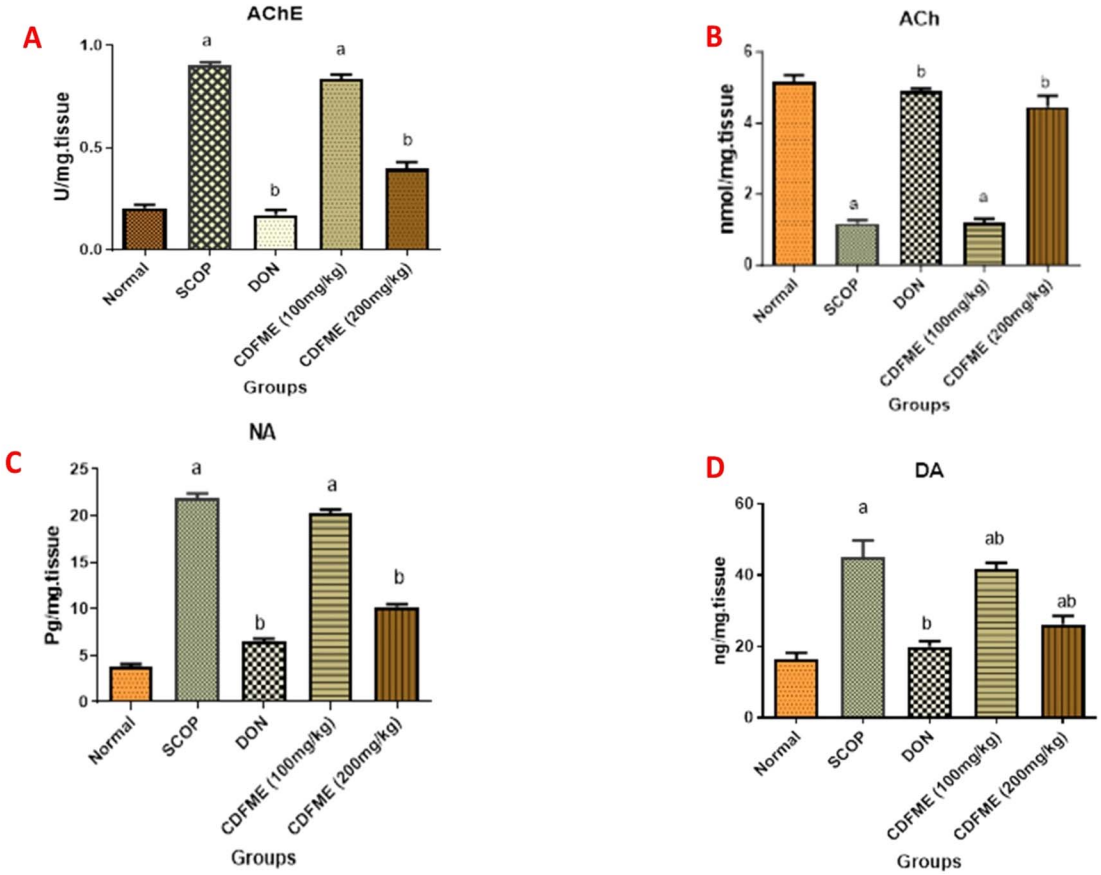

Fig. 4 Rat hippocampus levels of (A) AChE, (B) ACh, (C) NA, and (D) DA. Data are presented as mean ± SD ($n = 6$). Statistical analysis was done using one-way ANOVA, followed by Tukey's multiple comparisons test ($p < 0.05$). Letters "a" and "b" indicate significant differences compared to the normal control group and the SCOP control group, respectively. The analysis showed significant group differences (df between groups = [4], df within groups = [25], R^2 = [0.95, 0.99, 0.955, 0.988], respectively), with the 200 mg kg^{-1} of CDFME dose yielding a strong and positive effect on neurotransmitter levels associated with memory function.

rosmarinic acid,[67] were reported to have a potent anti-AChE effect. *p*-Coumaric acid mitigates LPS-induced brain damage and decreases AChE level in the brains of mice.[66] Coumarins have the potential to treat AD and enhance cognitive performance by blocking AChE.[75] Moreover, previous research showed that amino acids[76] and organic acids such as quinic acid[74] exhibited *in vitro* AChE inhibitory activity. Dietary polyunsaturated fatty acids[77] and choline in the diet[78] improved cholinergic transmission, increased ACh release in the aged brain, and inhibited AChE.

Several research works have emphasized the influence of classical neurotransmitter systems, like NA and DA, on cognitive processes such as concentration, learning, and memory.[8] Neurochemical changes in aging and AD involve neurotransmitter systems like adrenergic and dopaminergic. In order to preserve functional stability, endogenous neurotransmitter secretion normally stays in a harmonious ratio and at a specified level. According to earlier research, an increase in NA and DA levels leads to AD symptoms.[65] The association between AD progression and dysfunction in the noradrenergic system is not completely understood. An excess of NA may lead to production of toxic metabolites, contributing to disease progression.[79] Drugs increasing NA levels in early AD stages may cause adverse effects and worsen cognitive symptoms due to altered adrenergic receptor function, making the decrease of NA level a potential therapeutic goal.[79] Previous research suggested that SCOP increases NA and DA levels in both the cortex and hippocampus.[65]

As expected, in the SCOP control group, there was a significant increase in NA and DA levels by 481%, and 173%, respectively, compared to the normal control group (Table 3 and Fig. 4). DON decreased the elevated NA and DA levels by 70% and 55%, respectively, as compared with the SCOP control group. Likewise, as observed before for ACh, CDFME (200 mg kg^{-1}) induced a similar neuroprotective effect to DON, resulting in significant reductions in NA and DA levels compared to the SCOP control group by 53% and 41%, respectively. These results suggested that CDFME may improve memory and learning capacities by modulating the metabolic pathway of monoamine neurotransmitters. To gain additional insights on the phytoconstituents responsible for the bioactivity of CDFME, molecular docking, molecular dynamics, and molecular mechanics studies were conducted.

3.4.3 Molecular docking. The cholinesterase inhibitory activity of the 18 most abundant compounds in CDFME was compared to both DON and the co-crystallized inhibitor, as reference standards. Notably, the phenolic acids rosmarinic acid, caffeoyl-4′-hydroxyphenyllactate, and sebestenoid C, along with the lignan sagerinic acid, displayed high affinity for AChE with binding scores of −7.57, −7.39, −8.47, and −7.78 kcal mol^{-1}, respectively. These values were comparable to those obtained for DON (−8.13 kcal mol^{-1}) and the co-crystallized inhibitor (−7.88 kcal mol^{-1}). As these phenolic acids and lignan showed the best compromise between the abundance in CDFME, the affinity for AChE, and previous literature reports suggesting relevant neuroprotective properties, they were selected for further investigation in this part of our study.[80]

The 2D and 3D interactions, along with the binding positioning for these four compounds, are depicted in Table 4. The co-crystallized inhibitor of AChE was stabilized by binding to Ser200, Ala201, Gly118, and Gly119 amino acids. In contrast, rosmarinic acid formed one H-bond with Glu199 and one pi–H bond with Gly118. Moreover, caffeoyl-4′-hydroxyphenyllactate bound Gly118 and Tyr334 with pi-H and pi–pi bonds,

Table 4 3D interactions and binding positioning for rosmarinic acid, caffeoyl-4′-hydroxyphenyllactate, sebestenoid C, and sagerinic acid within the ACh binding pocket

Comp.	3D interactions	3D positioning
Rosmarinic acid	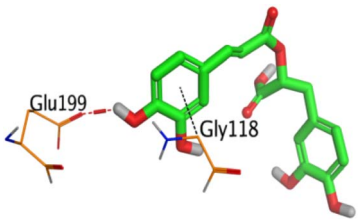	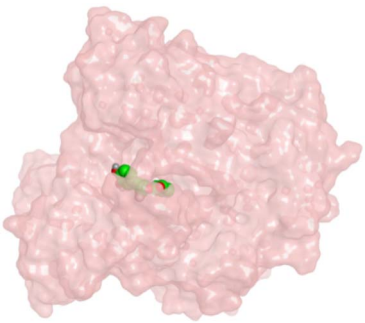
Caffeoyl-4′-hydroxyphenyllactate	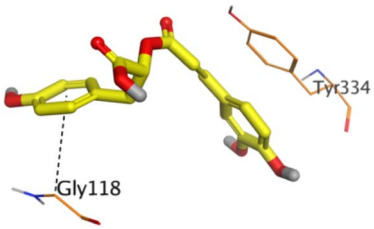	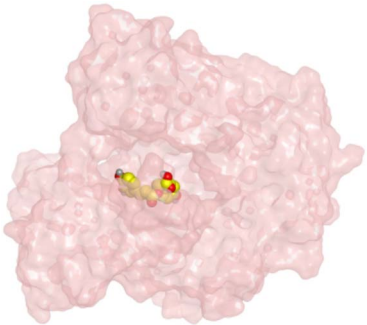
Sebestenoid C	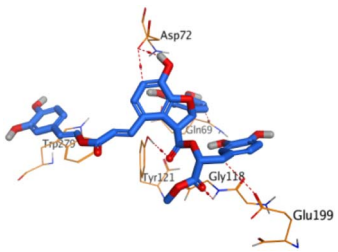	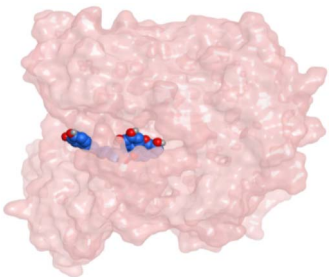
Sagerinic acid	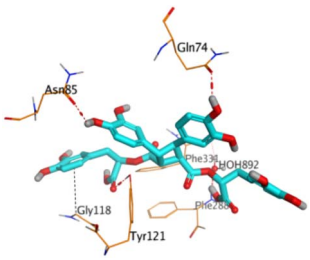	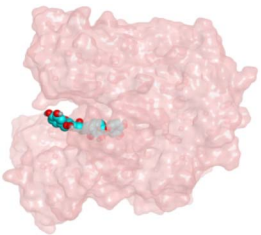

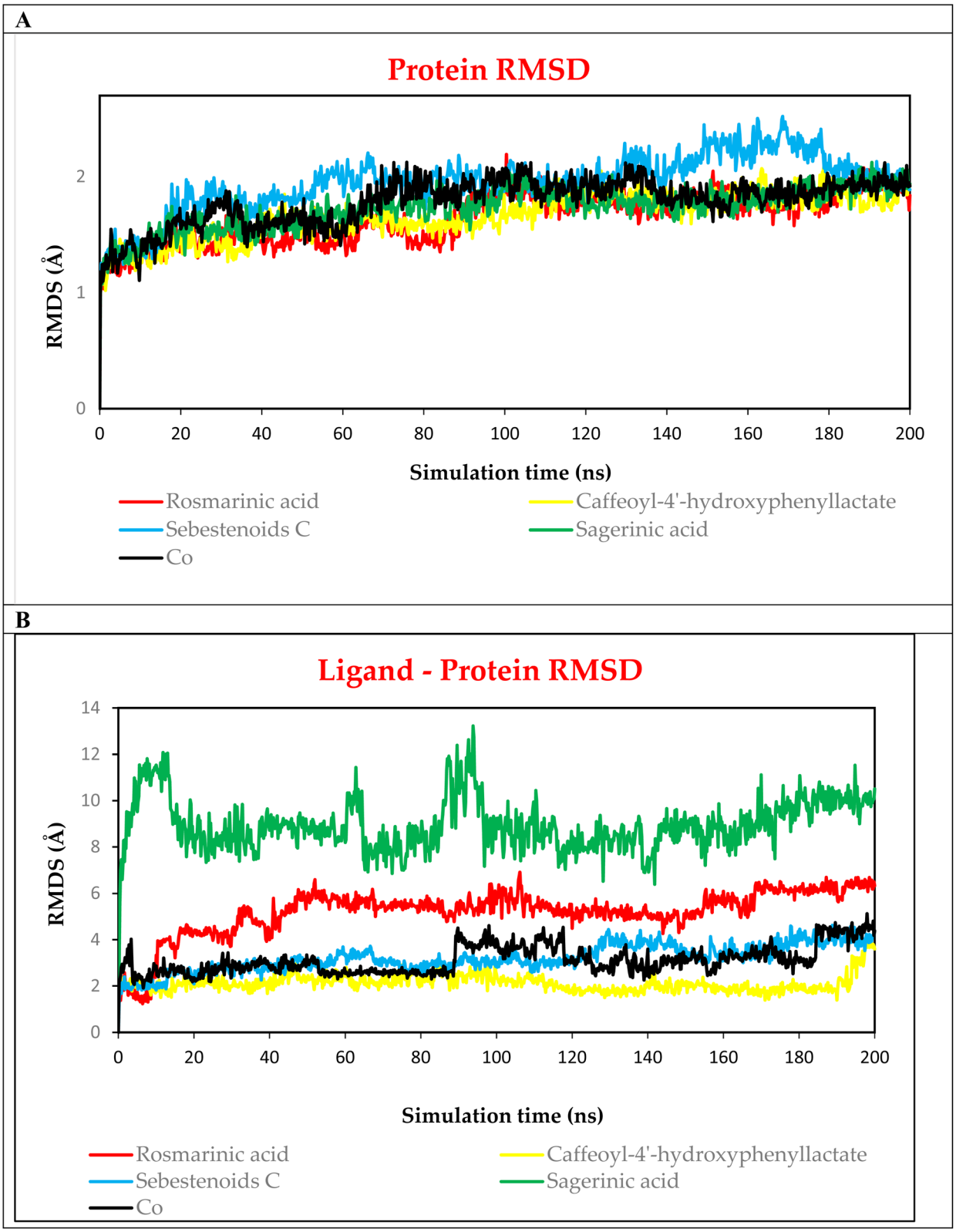

Fig. 5 (A) RMSD values of the complexes of the four selected compounds (rosmarinic acid, caffeoyl-4′-hydroxyphenyllactate, sebestenoid C, and sagerinic acid) and the co-crystallized inhibitor (DON) with the AChE receptor as a function of the simulation time (200 ns) (B) RMSD values of the ligand-protein bindings for the four selected compounds (rosmarinic acid, caffeoyl-4′-hydroxyphenyllactate, sebestenoid C, and sagerinic acid) and the co-crystallized inhibitor (DON) in the complex with the AChE receptor as a function of simulation time (200 ns).

respectively. Sebestenoid C formed six H-bonds with Gly118, Glu199, Gln69, Tyr121, and Asp72 (2), along with one pi–pi bond with Trp279. Finally, sagerinic acid bound through three H-bonds with Tyr121, Asn85, and Gln74. It also formed two H_2O-bridged H-bonds with Phe288 and Phe331 through the H_2O892 molecule, and one pi–H bond with Gly118. Based on the above and considering that these four compounds occupied the same binding pocket of the co-crystallized inhibitor, a promising antagonistic activity could be inferred (Table 4).

3.4.4 Molecular dynamics simulations. The complexes of the four selected compounds with the AChE target receptor (rosmarinic acid, caffeoyl-4′-hydroxyphenyllactate, sebestenoid C, and sagerinic acid-1OCE) were subjected to 200 ns molecular dynamics simulations to investigate their stabilities, using as a reference standard the co-crystallized inhibitor (DON) complex (Co-1OCE).

The RMSD of the examined protein complexes as a function of the simulation time was compared to their initial values to examine their exact stability. Throughout the simulations, the RMSD values consistently remained below 2.5 Å, indicating highly stable behaviors. With the exception of the sebestenoid C-1OCE complex, all other complexes exhibited RMSD values around 2 Å, closely resembling those of the Co-1OCE reference (Fig. 5A).

Additionally, the ligands' RMSD analysis was conducted to clarify the degree of stability for rosmarinic acid, caffeoyl-4′-hydroxyphenyllactate, sebestenoid C, and sagerinic acid compared to that of the co-crystallized inhibitor (DON) (Fig. 5B). The RMSD values for the four compounds fluctuated along the simulation time up to 7.2, 4, 4.5, and 13.5 Å, respectively, compared to the co-crystallized DON (4.8 Å). As can be observed in Fig. 5B, rosmarinic acid showed moderate stability, where it fluctuated gradually from the start up to 7.2 Å. Meanwhile, sagerinic acid showed the least stable behavior due to its large fluctuations, especially from 0 to 100 ns, reaching an average of about 12 Å. Notably, both caffeoyl-4′-hydroxyphenyllactate and sebestenoid C described the most stable behaviors, which were very close to those of the co-crystallized ligand. Specifically, caffeoyl-4′-hydroxyphenyllactate achieved the highest stability, with fluctuations lower than 4 Å. This value was slightly lower than the value for the co-crystallized DON (4.8 Å). The subsequent discussion provides a detailed analysis of the caffeoyl-4′-hydroxyphenyllactate-1OCE complex in comparison to the Co-1OCE reference standard.

3.4.4.1 Protein-ligand interactions analysis (histogram and heat map). Both the histogram and heat map of the caffeoyl-4′-hydroxyphenyllactate-1OCE complex were compared to those of the Co-1OCE (Fig. 6A and 7A, respectively). The histograms and heat maps of rosmarinic acid, sebestenoid C, and sagerinic

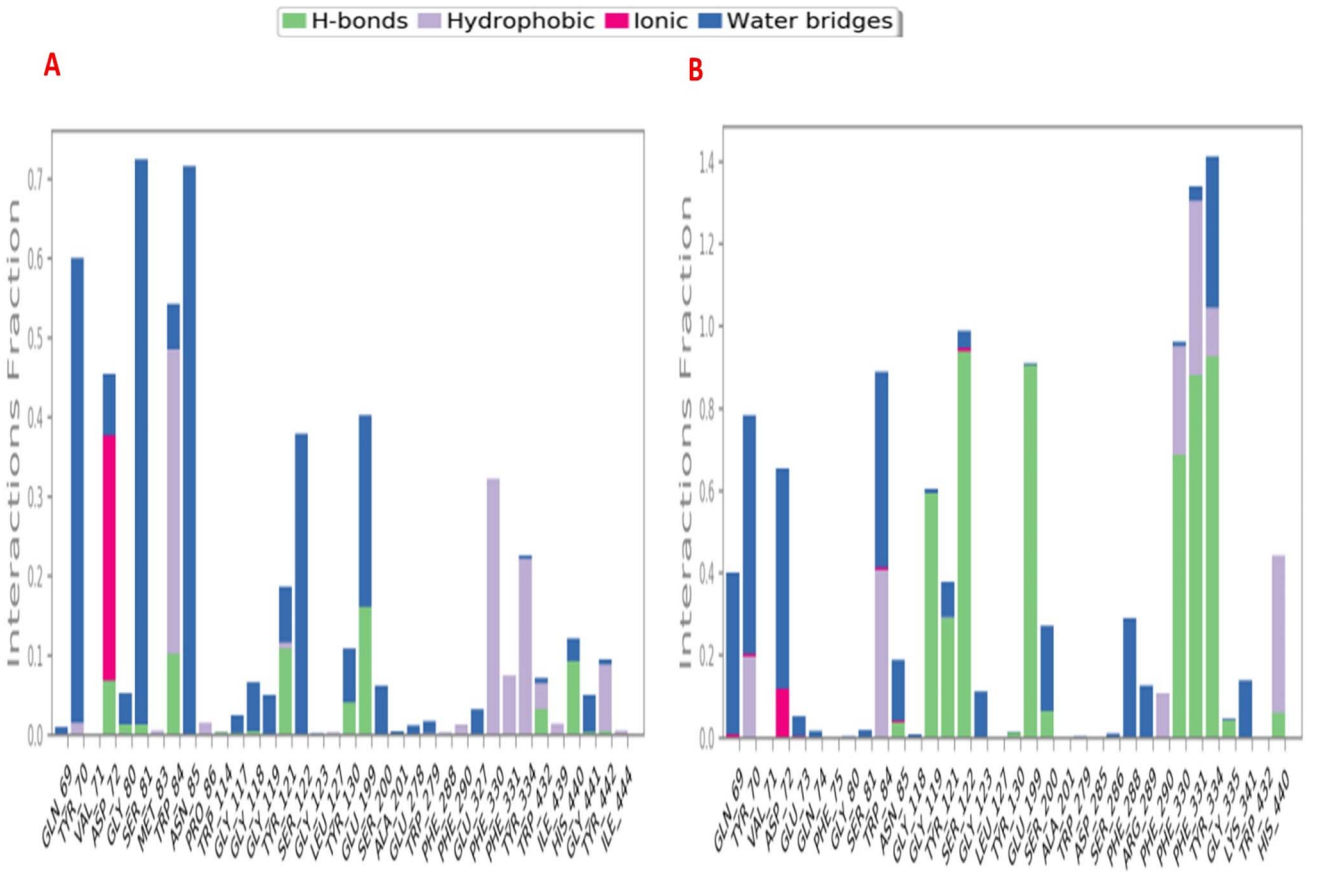

Fig. 6 Histograms of (A) caffeoyl-4′-hydroxyphenyllactate and (B) DON (Co) ligands within the binding site of AChE(1OCE) during the simulation time of 200 ns.

acid-1OCE complexes are provided as ESI (Fig. S22 and S23,† respectively).

Regarding the histogram of the caffeoyl-4′-hydroxyphenyllactate-1OCE complex (Fig. 6A), it was evident that Tyr334 and Phe331 were the most contributing amino acids from the AChE receptor to the interaction with caffeoyl-4′-hydroxyphenyllactate. Tyr334 showed 140% total interactions, in the form of H-bonds (100%), hydrophobic interactions (10%), and H_2O-bridges H-bonds (30%). Similarly, Phe331 described total interactions exceeding 130%, divided as H-bonds (90%), hydrophobic interactions (40%), and H_2O-bridges H-bonds (∼5%). Additionally, the heat map of caffeoyl-4′-hydroxyphenyllactate-1OCE complex (Fig. 7A) showed that both Tyr334 and Phe331 amino acids of the AChE binding pocket involved in the interactions with the caffeoyl-4′-hydroxyphenyllactate ligand throughout the 200 ns of the simulation (indicated by the dark orange color).

In contrast to these results, the histogram of the Co-1OCE complex (Fig. 6B) represented that Ser81, Asn85, and Tyr70 amino acids were the most prominent residues involved in interactions with the co-crystallized inhibitor of AChE. Their total interactions fractions were >70%, 70%, and 60%, respectively. Ser81 interactions were in the form of H_2O-bridges H-bonds (70%) and H-bonds (∼3%), while those of Asn85 were exclusively in the form of H_2O-bridges H-bonds (70%). As for Tyr70, its interactions were classified as H_2O-bridges H-bonds (58%) and hydrophobic bonds (∼2%). Additionally, the heat map of the Co-1OCE complex (Fig. 7B) highlighted that Ser81 interactions with the Co-1OCE throughout the 200 ns simulation, becoming more intense in the second half (>100 ns). On the other hand, Asn85 and Tyr70 showed more intense interactions from 30 to 200 ns of the simulation. Finally, Tyr70 interactions were clearer from 30 to about 185 ns of the simulation time.

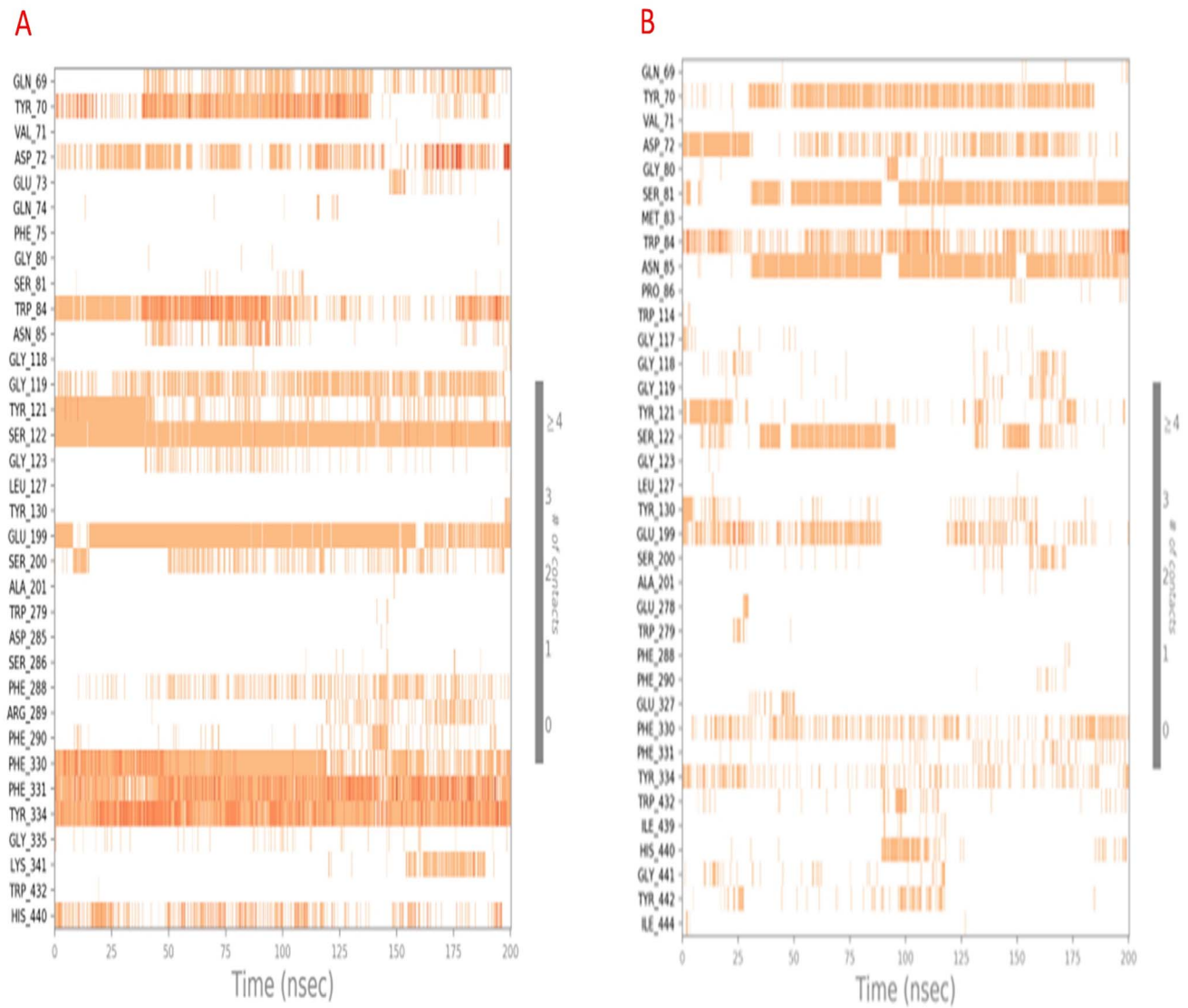

Fig. 7 Heat maps of (A) caffeoyl-4′-hydroxyphenyllactate and (B) DON (Co) ligands within the binding site of AChE(1OCE) during the simulation time of 200 ns.

Table 5 Prime MM-GBSA binding energies (kcal mol^{-1}) for the studied protein complexes (rosmarinic acid-1OCE, caffeoyl-4′-hydroxyphenyllactate-1OCE, sebestenoid C-1OCE, sagerinic acid-1OCE, and Co-1OCE)[a]

Complex	ΔG binding	Coulomb	Covalent	H-bond	Lipo	Bind packing	Solv_GB	VdW	SD
Rosmarinic acid-1OCE	−60.05	28.56	3.15	−3.07	−26.26	−3.99	−18.43	−40.01	10.84
Caffeoyl-4′-hydroxyphenyllactate-1OCE	−63.28	33.50	2.14	−3.91	−22.95	−3.37	−29.41	−39.27	10.27
Sebestenoid C-1OCE	−83.98	−42.86	7.32	−4.49	−36.76	−3.96	77.00	−80.22	15.98
Sagerinic acid-1OCE	−50.76	129.81	4.50	−2.80	−20.85	−3.10	−111.18	−47.14	8.73
Co-1OCE	−46.56	−49.49	1.55	−0.58	−19.30	0	63.05	−41.79	5.12

[a] Coulomb: coulomb energy; covalent: covalent binding energy; H-bond: hydrogen-bonding energy; Lipo: lipophilic energy; Solv_GB: generalized born electrostatic solvation energy; VdW: van der Waals energy; and SD: standard deviation.

3.4.5 Molecular mechanics. Complementary molecular mechanics calculations were conducted to complete the stability assessment of the different protein complexes. The average MM-GBSA binding energies for rosmarinic acid-1OCE, caffeoyl-4′-hydroxyphenyllactate-1OCE, sebestenoid C-1OCE, sagerinic acid-1OCE, and Co-1OCE complexes were calculated. The total energy (ΔG) and the contributions from different components to the total energy are summarized in Table 5.

As can be observed in Table 5, all the examined complexes showed superior ΔG binding energies compared to that of the co-crystallized inhibitor complex (−46.56 kcal mol^{-1}). Consistent with the findings from the molecular docking and molecular dynamics studies, both the caffeoyl-4′-hydroxyphenyllactate-1OCE and sebestenoid C-1OCE complexes presented the highest ΔG binding energies (−63.28 and −83.98 kcal mol^{-1}, respectively). Additionally, the contributions from different components to the total energy in all cases were very close or superior to those of the Co-1OCE complex. This suggested a very promising perspective regarding the AChE inhibitory potential of the examined compounds from CDFME, particularly the phenolic acids; caffeoyl-4′-hydroxyphenyllactate and sebestenoid C.

4. Conclusion

In light of the aforementioned findings, CDFME demonstrated the presence of valuable phenolic compounds, coumarins, essential amino acids, and phospholipids, which were reported to have a neuroprotective effect. *C. dichotoma* fruit extract exhibited a cognition-enhancing and neuromodulatory effect by reversing SCOP-induced learning and memory deficits in rats. The protective effect was observed by an increase in visual recognition in the behavioral test. Also, the treatment improved cholinergic neuronal activity by decreasing AChE and increasing ACh levels in the rat hippocampus. Moreover, it showed a correction of neurotransmitter imbalances. Additionally, molecular docking revealed that among the most abundant metabolites, rosmarinic acid, caffeoyl-4′-hydroxyphenyllactate, sebestenoid C, and sagerinic acid were found to show the highest binding affinity towards AChE with binding scores of −7.57, −7.38, −8.47, and −7.78 kcal mol^{-1}, respectively, compared to DON (−8.13 kcal mol^{-1}) and the co-crystallized inhibitor (−7.88 kcal mol^{-1}). Furthermore, molecular dynamics and molecular mechanics clarified that caffeoyl-4′-hydroxyphenyllactate-1OCE complex was the most stable one. Therefore, the study supports the use of CDFME in the food industries and pharmaceuticals for developing memory-enhancing nutraceuticals and functional foods. However, more detailed mechanistic studies are needed in the future to demonstrate cognitive function-enhancing effects of CDFME on other potential mechanisms involved in AD pathogenesis, such as inflammatory and glutamatergic pathways, and its antioxidant potential as well. Further research into bioassay-guided separation and quantification of potential active compounds in the fruit extract, as well as their therapeutic evaluation in AD, is advised. More detailed and conclusive *in vivo* and clinical studies are highly recommended to investigate the potential of. *C. dichotoma* fruit extract in treating patients with AD. As far as we are aware, our research is the first to characterize metabolic profile and investigate cognitive function-enhancing effects of *C. dichotoma* fruit extract.

Abbreviations

ACh	Acetylcholine
AChE	Acetylcholinesterase
AD	Alzheimer's disease
CDFME	*C. dichotoma* fruit methanolic extract
Co-1OCE	Co-crystallized ligand (inhibitor or DON) complex
DA	Dopamine
DI	Discrimination index
DON	Donepezil
ESI	Electrospray ionization
LC-QTOF-MS/MS	Liquid chromatography quadrupole time-of-flight mass spectrometry
MM-GBSA	Molecular mechanics with generalized Born and surface area solvation
NA	Noradrenaline
NORT	Novel object recognition test
RMSD	Root mean square deviation
SCOP	Scopolamine
TFC	Total flavonoids content
TPC	Total phenolics content

Data availability

The authors confirm that the data supporting the finding of this study are available within the article and or its ESI.†

Conflicts of interest

Authors declare no conflicts of interest.

Acknowledgements

Basma M. Eltanany would like to thank the Egyptian Ministry of Higher Education for funding her postdoctoral research stay at the Bioanalysis group of the University of Barcelona.

References

1 V. Singh, A. Kahol, I. P. Singh, I. Saraf and R. Shri, *J. Ethnopharmacol.*, 2016, **193**, 490–499.
2 I. M. Ayoub, M. Y. George, E. T. Menze, M. Mahmoud, M. Botros, M. Essam, I. Ashmawy, P. Shendi, A. Hany, M. Galal, M. Ayman and R. M. Labib, *Food Funct.*, 2022, **13**, 2253–2268.
3 S. Bhatia, R. Rawal, P. Sharma, T. Singh, M. Singh and V. Singh, *Curr. Neuropharmacol.*, 2021, **20**, 675–692.
4 Y. Ma, M. W. Yang, X. W. Li, J. W. Yue, J. Z. Chen, M. W. Yang, X. Huang, L. L. Zhu, F. F. Hong and S. L. Yang, *Front. Pharmacol.*, 2019, **10**, 1355.
5 K. Randhawa, V. Singh, S. Kaur, R. Kaur, S. Kumar and R. Shri, *Food Sci. Hum. Wellness*, 2021, **10**, 490–496.
6 S. Pruthi, K. Kaur, V. Singh and R. Shri, *Metab. Brain Dis.*, 2021, **36**, 901–910.
7 V. Singh, K. Kaur, S. Kaur, R. Shri, T. G. Singh and M. Singh, *J. Ethnopharmacol.*, 2022, **295**, 115438.
8 X. Pan, A. C. Kaminga, P. Jia, S. W. Wen, K. Acheampong and A. Liu, *Front. Aging Neurosci.*, 2020, **12**, 1–12.
9 H. Hussein, E. Mohsen, A. Abdelmonem and M. Abdel Kawy, *Egpt. J. Chem.*, 2023, **66**, 437–459.
10 D. Raghuvanshi, K. Sharma, R. Verma, D. Kumar, H. Kumar, A. Khan, M. Valko, S. Y. Alomar, S. H. Alwasel, E. Nepovimova and K. Kuca, *Biomed. Pharmacother.*, 2022, **153**, 113400.
11 M. Yizibula, Z. Wusiman, N. Abudouhalike and B. Maimaitiming, *Folia Neuropathol.*, 2021, **58**, 365–376.
12 G. Kendir, H. J. Bae, J. Kim, Y. Jeong, H. J. Bae, K. Park, X. Yang, Y. jin Cho, J. Y. Kim, S. Y. Jung, A. Köroğlu, D. S. Jang and J. H. Ryu, *BMC Complementary Med. Ther.*, 2022, **22**, 215.
13 H. M. Hussein, E. Mohsen, A. R. Abdelmonem, M. A. A. Kawy, A. A. Al-Karmalawy and R. A. El-Shiekh, *Egpt. J. Chem.*, 2024, **67**, 225–237.
14 R. Malik, S. Kalra, Pooja, G. Singh, Meenu, V. Gahlot, A. Kajal and Rimpy, *Brain Res.*, 2024, **1822**, 148616.
15 I. Y. Younis, M. S. Sedeek, A. F. Essa, A. M. Elgamal, B. M. Eltanany, Z. M. Goda, L. Pont, F. Benavente and E. Mohsen, *Food Chem.*, 2024, **465**, 141918.
16 A. M. Khalil, O. M. Sabry, H. El-Askary, S. M. El Zalabani, B. M. Eltanany, L. Pont, F. Benavente, A. F. Mohamed and N. M. Fayek, *BMC Complementary Med. Ther.*, 2024, **24**, 379.
17 H. M. El-Sayed, D. M. Rasheed, E. A. Mahrous, B. M. Eltanany, Z. M. Goda, L. Pont, F. Benavente and E. Abdel-Sattar, *J. Pharm. Biomed. Anal.*, 2025, **252**, 116512.
18 A. M. Otify, S. A. ElBanna, B. M. Eltanany, L. Pont, F. Benavente and R. M. Ibrahim, *Food Res. Int.*, 2023, **172**, 113178.
19 N. M. Shofian, A. A. Hamid, A. Osman, N. Saari, F. Anwar, M. S. P. Dek and M. R. Hairuddin, *Int. J. Mol. Sci.*, 2011, **12**, 4678–4692.
20 E. Attard, *Cent. Eur. J. Biol.*, 2013, **8**, 48–53.
21 M. Kiranmai, C. B. Mahendra Kumar and M. Ibrahim, *Res. J. Pharm. Biol. Chem. Sci.*, 2011, **2**, 254–261.
22 R. M. Ibrahim, B. Eltanany, L. Pont, F. Benavente, S. AbdelSalam ElBanna and A. M. Otify, *Food Res. Int.*, 2023, **168**, 112742.
23 A. Ennaceur and J. Delacour, *Behav. Brain Res.*, 1988, **31**, 47–59.
24 N. A. Shaif, D. H. Chang, D. Cho, S. Kim, D. B. Seo and I. Shim, *Biomedicines*, 2018, **6**, 108.
25 M. F. Elshal, N. M. Eid, I. El-Sayed, W. El-Sayed and A. A. Al-Karmalawy, *Pharm. Sci.*, 2021, **28**, 76–85.
26 M. Khattab and A. A. Al-Karmalawy, *Future Med. Chem.*, 2021, **13**, 1623–1638.
27 A. A. Elmaaty, K. M. Darwish, A. Chrouda, A. A. Boseila, M. A. Tantawy, S. S. Elhady, A. B. Shaik, M. Mustafa and A. A. Al-Karmalawy, *ACS Omega*, 2021, **7**, 875–899.
28 M. A. Ragab, W. M. Eldehna, A. Nocentini, A. Bonardi, H. E. Okda, B. Elgendy, T. S. Ibrahim, M. M. Abd-Alhaseeb, P. Gratteri, C. T. Supuran, A. A. Al-Karmalawy and M. Elagawany, *Eur. J. Med. Chem.*, 2023, **250**, 115180.
29 A. M. El-Naggar, A. M. A. Hassan, E. B. Elkaeed, M. S. Alesawy and A. A. Al-Karmalawy, *Bioorg. Chem.*, 2022, **123**, 105770.
30 M. M. Hammoud, M. Khattab, M. Abdel-Motaal, J. Van der Eycken, R. Alnajjar, H. Abulkhair and A. A. Al-Karmalawy, *J. Biomol. Struct. Dyn.*, 2022, **41**, 5199–5216.
31 D. T. Ayele, M. L. Akele and A. T. Melese, *BMC Chem.*, 2022, **16**, 30.
32 A. M. Khalil, O. M. Sabry, H. I. El-Askary, S. M. El Zalabani, B. M. Eltanany, L. Pont, F. Benavente, A. Elshewy and N. M. Fayek, *Phytochem. Anal.*, 2024, **35**, 1–18.
33 T. Cheng, J. Ye, H. Li, H. Dong, N. Xie, N. Mi, Z. Zhang, J. Zou, H. Jin and W. Zhang, *RSC Adv.*, 2019, **9**, 8714–8727.
34 S. Yaermaimaiti, T. Wu and H. A. Aisa, *Ind. Crops Prod.*, 2021, **172**, 113977.
35 N. P. Araujo, H. S. Arruda, F. N. dos Santos, D. R. de Morais, G. A. Pereira and G. M. Pastore, *Food Res. Int.*, 2020, **137**, 109556.
36 J. A. B. Peixoto, G. Álvarez-Rivera, A. S. G. Costa, S. Machado, A. Cifuentes, E. Ibáñez, M. B. P. P. Oliveira and R. C. Alves, *Antioxidants*, 2023, **12**, 251.
37 L. Zhu, S. Ma, K. Li, P. Xiong and W. Cai, *Molecules*, 2022, **27**, 2631.
38 M. Kim, J. Y. Kim, H. S. Yang, J. S. Choe and I. G. Hwang, *Antioxidants*, 2021, **10**, 1208.
39 J. Dai, A. Sorribas, W. Y. Yoshida and P. G. Williams, *Phytochemistry*, 2010, **71**, 2168–2173.
40 K. Kramberger, D. Barlič-Maganja, D. Bandelj, A. Baruca Arbeiter, K. Peeters, A. Miklavčič Višnjevec and Z. J. Pražnikar, *Metabolites*, 2020, **10**, 403.

41 K. Niaz, M. A. Nawaz, S. Pervez, U. Younas, I. Shah and F. Khan, *S. Afr. J. Bot.*, 2022, **144**, 437–447.
42 B. S. Zhumakanova, I. Korona-Głowniak, K. Skalicka-Woźniak, A. Ludwiczuk, T. Baj, K. K. Wojtanowski, A. Józefczyk, K. A. Zhaparkulova, Z. B. Sakipova and A. Malm, *Molecules*, 2021, **26**, 3193.
43 P. López-Rojas, Á. Amesty, M. Guerra-Rodríguez, Y. Brito-Casillas, B. Guerra, L. Fernández-Pérez and A. Estévez-Braun, *Pharmaceuticals*, 2022, **15**, 1–30.
44 J. Simayi, A. Abulizi, M. Nuermaimaiti, N. Khan, S. Hailati, M. Han, Z. Talihati, K. Abudurousuli, N. Maihemuti, M. Nuer, W. Zhou and A. Wumaier, *Biomed Res. Int.*, 2022, **2022**, 4176235.
45 L. R. Fernández, A. Cirigliano, M. P. Fabani, B. Lima, S. Alberti, F. Kramer, A. A. Tapia, G. Cabrera, J. A. Palermo and M. Sánchez, *Planta Med.*, 2013, **79**, 1724–1729.
46 Y. H. Lee, B. Kim, S. Kim, M. S. Kim, H. Kim, S. R. Hwang, K. Kim and J. H. Lee, *J. Food Drug Anal.*, 2017, **25**, 776–788.
47 S. A. S. da Silva, A. L. Souto, M. de F. Agra, E. V. L. Da-Cunha, J. M. Barbosa-Filho, M. S. da Silva and R. Braz-Filho, *Arkivoc*, 2004, 54–58.
48 A. Trifan, E. Wolfram, N. Esslinger, A. Grubelnik, K. Skalicka-Woźniak, M. Minceva and S. V. Luca, *Phytochem. Anal.*, 2021, **32**, 482–494.
49 K. N. Venugopala, V. Rashmi and B. Odhav, *Biomed Res. Int.*, 2013, **2013**, 963248.
50 K. Wang, J. Tian, Y. Li, M. Liu, Y. Chao, Y. Cai, G. Zheng and Y. Fang, *ACS Omega*, 2021, **6**, 17045–17057.
51 M. J. Oza and Y. A. Kulkarni, *J. Pharm. Pharmacol.*, 2017, **69**, 755–789.
52 N. Guo, S. Zhang, M. Gu and G. Xu, *Crop J.*, 2021, **9**, 530–542.
53 Z. N. Ling, Y. F. Jiang, J. N. Ru, J. H. Lu, B. Ding and J. Wu, *Signal Transduct. Target. Ther.*, 2023, **8**, 345.
54 F. Zhang, B. Li, Y. Wen, Y. Liu, R. Liu, J. Liu, S. Liu and Y. Jiang, *Pharm. Biol.*, 2022, **60**, 1349–1364.
55 Z. Li, Z. Tu, H. Wang and L. Zhang, *Molecules*, 2020, **25**, 4507.
56 I. M. Abu-Reidah, M. S. Ali-Shtayeh, R. M. Jamous, D. Arráez-Román and A. Segura-Carretero, *Food Chem.*, 2015, **166**, 179–191.
57 Z. T. Abdel Shakour, R. H. El-Akad, A. I. Elshamy, A. E.-N. G. N. G. El Gendy, L. A. Wessjohann and M. A. Farag, *Food Chem.*, 2022, **399**, 133948.
58 R. Tanvir, A. Javeed and Y. Rehman, *FEMS Microbiol. Lett.*, 2018, **365**, fny114.
59 R. Gevrenova, G. Zengin, K. I. Sinan, E. Yıldıztugay, D. Zheleva-Dimitrova, C. Picot-Allain, M. F. Mahomoodally, M. Imran, S. Dall'acqua and S. Dall'acqua, *Antioxidants*, 2021, **10**, 1180.
60 A. Masyita, R. Mustika Sari, A. Dwi Astuti, B. Yasir, N. Rahma Rumata, T. Bin Emran, F. Nainu and J. Simal-Gandara, *Food Chem. X*, 2022, **13**, 100217.
61 F. Han, Y. Li, X. Mao, R. Xu and R. Yin, *MASS Spectrom.*, 2016, **51**, 363–368.
62 E. A. Mahrous, A. H. Elosaily, A. A. A. Salama, A. M. Salama and S. M. El-Zalabani, *Plants*, 2022, **11**, 218.
63 B. Lin, S. Guo, X. Hong, X. Jiang, H. Li, J. Li, L. Guo, M. Li, J. Chen, B. Huang, Y. Xu and M. G. Ferraro, *Evid. Based Complement. Altern. Med.*, 2022, **2022**, 1322751.
64 M. E. Hussein, O. G. Mohamed, A. M. El-Fishawy, H. I. El-Askary, A. A. Hamed, M. M. Abdel-Aziz, R. Alnajjar, A. Belal, A. M. Naglah, A. A. Almehizia, A. A. Al-Karmalawy, A. Tripathi and A. S. El Senousy, *Plants*, 2022, **11**, 3286.
65 S. Bhuvanendran, Y. Kumari, I. Othman and M. F. Shaikh, *Front. Pharmacol.*, 2018, **9**, 665.
66 G. Caruso, J. Godos, A. Privitera, G. Lanza, S. Castellano, A. Chillemi, O. Bruni, R. Ferri, F. Caraci and G. Grosso, *Nutrients*, 2022, **14**, 819.
67 S. Habtemariam, *Int. J. Mol. Sci.*, 2018, **19**, 458.
68 H. Suzuki, D. Yamashiro, S. Ogawa, M. Kobayashi, D. Cho, A. Iizuka, M. Tsukamoto-Yasui, M. Takada, M. Isokawa, K. Nagao and Y. Fujiwara, *Front. Nutr.*, 2020, **7**, 586166.
69 R. Tao, S. Huang, J. Zhou, L. Ye, X. Shen, J. Wu and L. Qian, *J. Nutr.*, 2022, **152**, 889–898.
70 L. Taoro-González, D. Pereda, C. Valdés-Baizabal, M. González-Gómez, J. A. Pérez, F. Mesa-Herrera, A. Canerina-Amaro, H. Pérez-González, C. Rodríguez, M. Díaz and R. Marin, *Int. J. Mol. Sci.*, 2022, **23**, 7430.
71 Z. Bao, P. Zhang, J. Chen, J. Gao, S. Lin and N. Sun, *J. Funct. Foods*, 2020, **69**, 103948.
72 P. Świt, A. Pollap and J. Orzeł, *Top. Curr. Chem.*, 2023, **381**, 16.
73 S. C. Jee, K. M. Lee, M. Kim, Y. J. Lee, S. Kim, J. O. Park and J. S. Sung, *Int. J. Mol. Sci.*, 2020, **21**, 9202.
74 S. Ahmed, S. T. Khan, M. K. Zargaham, A. U. Khan, S. Khan, A. Hussain, J. Uddin, A. Khan and A. Al-Harrasi, *Biomed. Pharmacother.*, 2021, **139**, 111609.
75 R. Joshi, *ChemistrySelect*, 2023, **8**, 202303861.
76 Z. Kovarik, Z. Radić, B. Grgas, M. Škrinjarić-Špoljar, E. Reiner and V. Simeon-Rudolf, *Biochim. Biophys. Acta*, 1999, **1433**, 261–271.
77 L. M. Willis, B. Shukitt-Hale and J. A. Joseph, *Genes Nutr.*, 2009, **4**, 309–314.
78 A. M. Wiedeman, S. I. Barr, T. J. Green, Z. Xu, S. M. Innis and D. D. Kitts, *Nutrients*, 2018, **10**, 1513.
79 I. L. Gutiérrez, C. Dello Russo, F. Novellino, J. R. Caso, B. García-Bueno, J. C. Leza and J. L. M. Madrigal, *Int. J. Mol. Sci.*, 2022, **23**, 6134.
80 M. Tavan, P. Hanachi, M. de la Luz Cádiz-Gurrea, A. Segura Carretero and M. H. Mirjalili, *Neurochem. Res.*, 2024, **49**, 306–326.